Journal of Cardiovascular Magnetic Resonance (2007) **9,** 827–843

ISSN: 1097-6647 print / 1532-429X online
DOI: 10.1080/10976640701693766

informa
healthcare

Molecular Imaging by Cardiovascular MR

Tillmann Cyrus, MB, MD, Gregory M. Lanza, MD, PhD, and **Samuel A. Wickline, MD**

Division of Cardiology, Washington University School of Medicine, St. Louis, Missouri, USA

ABSTRACT

Do molecularly-targeted contrast agents have what it takes to usher in a paradigm shift as to how we will image cardiovascular disease in the near future? Moreover, are non-invasive vulnerable plaque detection and preemptive treatments with these novel nanoparticulate agents within reach for clinical applications?

In this article, we attempt to make a compelling case for how the advent of molecularly-targeted nanoparticle technology may change the way we detect atherosclerotic lesions, determine their clinical significance and even provide non-invasive treatments. Focusing on imaging with cardiovascular MR, an overview of the latest developments in this rapidly evolving field of so-called "intelligent" contrast agents that are able to interrogate the vascular wall and various complementary advanced imaging technologies are presented.

After decades of observing lumenal obstructions and judging stenosis grades based on contrast deficits, the focus is shifting to determination of the characteristics of the vascular wall. This paradigm shift is based on the increasingly recognized relevance of the vulnerable plaque, which is implicated in many acute coronary events deriving from vascular plaques that are not considered clinically significant by lumenal angiography.

We have learned that significant atherosclerotic disease may exist without compromising the arterial lumen (1) and that most acute coronary syndromes are the result of sudden lumenal thrombosis, which forms on a ruptured or eroded plaque and to lesser degrees on calcified plaques (2–5). Furthermore, age and gender disparities regarding myocardial infarctions and sudden death have been observed for plaque rupture and erosion as underlying etiology. For example, plaque erosion causes most of the acute coronary thrombi in premenopausal women, while plaque rupture is more prevalent in postmenopausal women (6). Both such plaques may not represent significant lumenal obstructions as determined with digital subtraction angiography, CT angiography, or MR angiography. In fact, in autopsy studies, approximately 75% of culprit arteries showed <75% cross-sectional lumenal narrowing (7). However, both have distinct characteristics that are amenable to enhanced imaging modalities. The classic form of vulnerable plaque consists of a necrotic and lipid core, overlaid by a thin macrophage infiltrated fibrous cap <65 μm thick (3), but many variations exist. The plaque prone to erosion may have endothelial cell damage resulting in increased platelet adhesion over a period of time prior to complete erosion, providing a window of opportunity for detection before thrombotic vascular occlusion occurs. Importantly, many plaque ruptures leading to acute coronary syndromes occur in plaques that have previously ruptured and healed (8). These plaques contain a hemorrhagic core, which may show distinct features for advanced imaging. The identification of these respective characteristics of atherosclerotic plaques will be important to provide a *risk assessment* for individual plaques in individual patients, and, thus, guide treatment decisions that finally may decrease the occurrence of acute cardiovascular syndromes. In the quest to interrogate the vascular wall several invasive technologies have been developed with intravascular ultrasound being used in clinical practice to varying degrees, while others such as optical coherence tomography, angioscopy, near-infrared tomography and other thermographic measurements, and intravascular MRI are largely being used for research applications and select clinical trials. All of these technologies are invasive, require highly trained staff, are expensive, and cannot provide therapy. Thus, widespread clinical routine application faces significant hurdles. Molecularly targeted

Received 1 May 2007; accepted 26 July 2007.
This work was support by an American Heart Association grant awarded to Dr. Cyrus (0735067N).
Keywords: MRI, Nanoparticle, Molecular Targeting, Contrast Agent, Vulnerable Plaque, Atherosclerosis
Correspondence to:
Samuel A. Wickline, MD
Washington University School of Medicine
4320 Forest Park Avenue
CORTEX Bldg. Suite 101, Campus Box 8215
Saint Louis, MO 63108
tel: 314-454-8811
fax: 314-454-5265
email: saw@howdy.wustl.edu

nanoparticle technology on the other hand is being developed to yield "*intelligent*" *contrast agents*, which are injected systemically or locally and selectively accumulate in vulnerable plaques. Non-invasive imaging will detect the labeled nanoparticles and could be performed in any hospital equipped with single-photon-emission computed tomography (SPECT), CT, or MR.

This article focuses on molecular imaging with MRI, but brief mention shall be made regarding other very valuable imaging technologies, including nuclear imaging and CT. Specific strengths of nuclear imaging are the detection of metabolic and (patho-)physiologic processes and the high sensitivity and specificity in the detection of sparse epitopes. Positron-emission tomography (PET) and SPECT are capable of high resolution sufficient to generate useful information of targets that are too small to be detected or interpreted regarding their significance, with MRI or CT. Conversely, MRI and CT provide high spatial resolution and anatomical correlation. For these reasons many applications are being developed that use nuclear imaging in conjunction with either CT or MRI. Accordingly, many nanoparticulate agents are being developed for dual-imaging purposes. Several of the nuclear/MRI dual-agents are described below. However, for further in-depth study regarding nuclear imaging and developments in molecular nuclear imaging, the reader is referred to two excellent review articles, which have been recently published (9,10).

DIAGNOSTIC MR MOLECULAR IMAGING OF ATHEROSCLEROSIS

Emphasizing its true character of a systemic inflammatory disease, atherosclerotic lesions can be found throughout the arterial tree. Yet, not all lesions are equal and location does matter. Thus, carotid artery lesions are prone to form thrombi on the surface and embolize into cranial arteries causing strokes (11–16), while femoral and other peripheral arteries achieve clinical significance largely through slow but continuous vascular occlusion (17–19). Aortic lesions can cause embolic phenomena (20–22). However, most clinically recognized events are related to instrumentation (23). Coronary arteries can be diseased with atherosclerotic lesions prone to all mechanisms of acute or slow vascular occlusion (24). They are an important site for molecular imaging of vulnerable plaques since these have been shown to be a significant source of acute myocardial infarctions (25–27). While slowly occluding lesions eventually also cause heart attacks, many of these are detected in time since they lead to symptoms in more than half of cases, eventually may cause ischemic changes on various forms of stress testing and can be detected with current angiography techniques. Vulnerable plaques often occur in the proximal and middle parts of coronary arteries making them more amenable to non-invasive imaging modalities (28). Breath-hold maneuvers and ECG-gating techniques have significantly diminished the impact of motion artifacts on obtaining non-invasive images concerning lumenal patency. However, the interrogation of small non-lumen compromising vulnerable plaques requires either invasive imaging or the addition of targeted contrast agents such as molecularly targeted nanoparticles. For human applications, molecular imaging of carotid and coronary arteries will be of greatest significance and supplementing MRI techniques are improving at rapid pace. While these efforts are ongoing, many of the animal trials to evaluate and refine targeted nanoparticle technology are conducted targeting and imaging plaque in carotid, aortic, and femoral arteries to minimize motion artifacts and improve reproducibility in experimental settings which also decreases animal usage.

Since there is overlap of different morphologies of atherosclerotic plaques in the various arterial beds, strategies to target specific types of atherosclerotic plaque for molecular imaging are described here. Other than angiography, which determines lumenal obstruction by contrast deficits, molecularly targeted nanoparticulate agents can interrogate the vessel from the lumenal side, detecting fibrin, or cellular markers on the endothelial or injured intimal surface, such as VCAM-1 (Figure 1). They can reach molecular targets deep within the vascular intima and media, such as integrins or by being shuttled into these layers following phagocytosis by macrophages or while linked to lipids. Finally, they can approach through vasa vasorum in the outer vascular wall to reach targets in angiogenic vessels which are feeding the developing plaque. Thus, molecularly targeted nanoparticles offer numerous opportunities to image atherosclerotic plaque and non-invasively provide risk assessments regarding the vulnerability of individual atheroma. To accomplish these numerous tasks, a wide variety of nanoparticles has been developed for imaging purposes, including stem cell-labeling and nanoparticles with dual (targeting & imaging) and triple (targeting & imaging & drug delivery) functionality (Figure 2).

MOLECULAR IMAGING OF PLAQUE EROSION OR RUPTURE

The interruption of the endothelial layer due to plaque erosion or focal rupture causes fibrin deposition (5, 29). The detection of this event is appealing for two reasons. One, acute vascular occlusion due to ongoing thrombus formation may ensue in the short term, and second, hemorrhage into the plaque is known to contribute to the growth of plaques, which often become vulnerable again in the long term (30, 31). Both these events may be prevented as a result of treatment decisions derived from molecular imaging of fibrin deposition. Early work to develop MR detectable nanoparticles that target fibrin dates back to the 1990s when paramagnetic perfluorocarbon nanoparticles were formulated with a ligand consisting of an antibody fragment highly specific for cross-linked fibrin peptide domains (32, 33). In those experiments, thrombi, formed *in situ* in canine carotid arteries, were detectable within 30 minutes after exposure to the fibrin targeted nanoparticles. Perfluorocarbon nanoparticles have a nominal diameter of 250 nm, consist of a liquid perfluorocarbon core and are encapsulated by a phospholipid monolayer which can carry > 90,000 Gd atoms per particle, thus improving T1-weighted contrast enhancement. In experiments using particles carrying >50,000 Gd atoms, dramatic T1-weighted

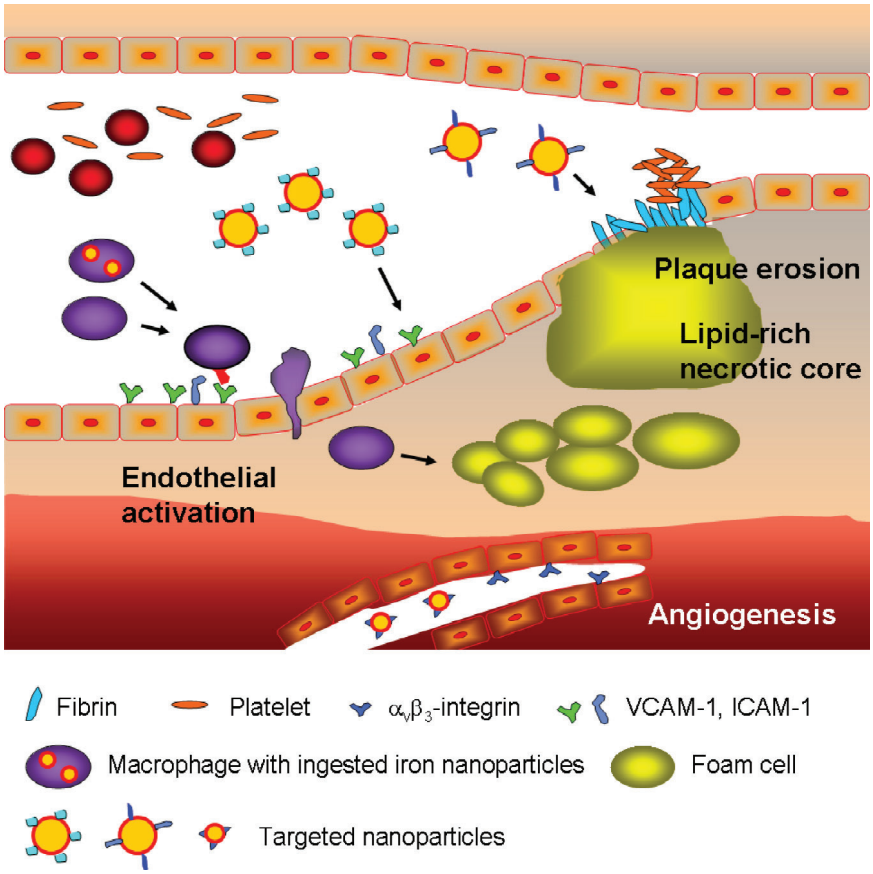

Figure 1. Illustration of molecular targets for CMR imaging. Atherogenesis ranging from endothelial activation (left) through atheroma development to thrombosis (right). Three different strategies are depicted. 1. Utilizing changes on the inner vascular surface throughout atherogenesis, nanoparticles can be formulated to target adhesion molecules such as ICAM-1 and VCAM-1, which are expressed during endothelial activation (early) or fibrin, which is expressed during endothelial injury (later). 2. Atherogenesis in the intima and media can be interrogated using macrophages that are loaded with nanoparticles such as iron-containing particles *in vitro* or *in vivo*. Other strategies can be utilized, e.g. HDL-like nanoparticles that migrate into the media (not depicted). 3. Angiogenesis supports advanced plaque growth. The angiogenic vessels sprout through the adventitia and typically express the $\alpha_v\beta_3$-integrin, which can be targeted with nanoparticles.

contrast enhancement in gradient-echo images was shown *in vivo* for nanoparticle targeted thrombi in the external jugular vein of dogs, and *ex vivo* for human endarterectomy specimen (34) (Figure 3).

Another approach to detect thrombi has utilized phage display methods to produce fibrin-targeted gadolinium-labeled peptides. These peptides carry 4 Gd atoms each and, thus, require accumulation of sufficient quantities at the target site for imaging. One such peptide, EP-1873, allowed the MR detection of "hot spots" in the subrenal aorta in a model of atherosclerotic NZW rabbits with induced plaque rupture within 30 minutes after systemic injection (35). Histological correlation confirmed all thrombi seen on MRI and no thrombi were detected by MRI or histology in control animals. The same fibrin-binding contrast agent was subsequently shown to facilitate MR imaging of thrombosis in a porcine model of coronary thrombus and in-stent thrombosis (36). A newer generation fibrin-specific small peptide with 4 Gd-chelate moieties, EP-2104R, binds selectively to fibrin without binding to circulating fibrinogen. This compound allowed the selective visualization of left atrial clots in a porcine model (37). This fibrin-targeted peptide has also been superior to non-contrast MRI and Gd-DTPA injection in targeting carotid artery thrombus *in vivo* (38). In this model, carotid artery thrombosis was induced by external injury and stasis in rabbits and T1-weighted MRI performed with a 1.5T system. Acute thrombi were as readily detected as chronic thrombi (i.e., >4 weeks after induction) and contrast to noise ratio was enhanced for both non-occlusive and occlusive thrombi.

Recently, chemical exchange saturation transfer (CEST) agents have received increased attention due to their ability to create stronger signal than conventional MR contrast agents. These agents contain exchangeable protons, which transfer magnetization to the strong signal of bulk water when they are irradiated at their resonance frequency. Thus, they can be switched on and off. This technology was initially explored in the 1990s (39–41) and has recently been employed for targeted nanoparticles

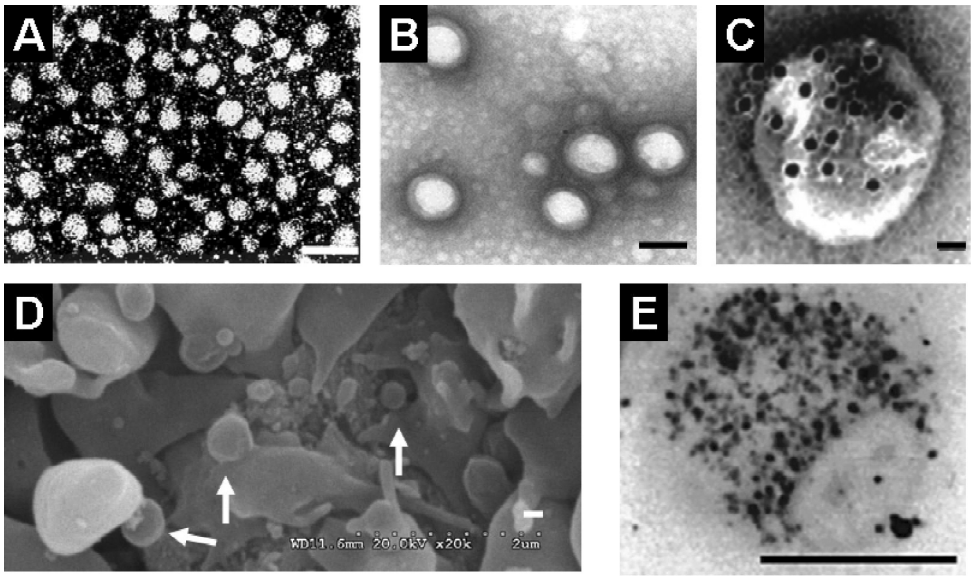

Figure 2. SEM images depicting size-variability of nanoparticulate agents used for CMR. (A) Example of an USPIO agent (ultra small particle of iron-oxide). Electron-microscopic appearance of magnetite particles with a mean diameter of 8.7 nm. Scale bar: 30 nm. Modified reprint with permission(151). (B) Biodegradable polymer nanoparticle. Shown here, poly ($_{D,L}$-lactide-*co*-glycolide) (PLGA) nanoparticles containing plasmid DNA. Mean particle diameter ~100 nm. Scale bar: 100 nm. Modified reprint with permission(152). (C) A single plasmid DNA-carrying liposome with receptor-specific monoclonal antibodies on the surface. Conjugates of a secondary antibody and 10 nm gold particles (black irregular structures on the liposome) have bound to some of monoclonal membrane-bound antibodies. Average liposome diameter ~40 nm. Scale bar: 20 nm. Modified reprint with permission(153). (D) $\alpha_v\beta_3$-integrin-targeted perfluorocarbon nanoparticles adherent to epitopes in balloon-angioplasty-injured vascular endothelium (arrows). Mean particle size: 250 nm. Scale bar: 200 nm. (Cyrus/Lanza 2007). (E) Single human mesenchymal stem cell which was targeted with magneto-dendrimers. Depicted is the non-nuclear location of the iron-particles. Scale bar: 20 nm. Modified reprint with permission (154).

using liposomes LIPOCEST (42, 43) and other paramagnetic nanoparticles PARACEST (44, 45). The CEST effect is based on the slow magnetization transfer from certain protons that are tightly bound to molecules such as lipids and proteins (41, 46). These low-molecular contrast agents contain labile protons (mostly in -NH and -OH groups), which can be selectively pre-saturated when tightly bound to certain lipids and proteins. This saturation can then be transferred to the signal of the bulk of the water, leading to a decrease in bulk water intensity. Chemical exchange rate and chemical shift are the most important factors to be considered in the generation of exogenous CEST agents. The chemical exchange rate should be as large as possible to enhance the CEST effect but must remain in the slow to intermediate exchange rate domain to ensure that a small spectral difference between the surrounding water and the CEST agent is maintained (40). At the same time, a large chemical shift between the water and the proton exchange site on the CEST agent is preferable since the chemical shift is positively related to the exchange rate, i.e., the larger the chemical shift between the water and the contrast agent, the greater the exchange rate without reaching the fast exchange limit.

An example for improved detection of fibrin with a novel PARACEST agent was recently shown when perfluorocarbon nanoparticles were formulated with an anti-fibrin antibody and targeted to fibrin clots *in vitro* (44). Spectroscopy (4.7T) of these PARACEST nanoparticles revealed a bound water peak at 52 ppm and produced >10% signal enhancement (Figure 4). Targeted PARACEST agents are particularly interesting because of the ability to switch the contrast on and off through the pulse sequence parameters of the MRI scanner. Thus, the collection of pre-contrast images for comparative purposes becomes less important. Other PARACEST agents have recently been reviewed (47).

MOLECULAR IMAGING OF THE ACTIVATED ENDOTHELIUM

One of the earliest events in the genesis of an atherosclerotic lesion is the overexpression of adhesion molecules secondary to exposure to inflammatory cytokines (48–51). Adhesion molecules important to this inflammatory response include E-selectin, which is involved in the rolling of leukocytes along the endothelium, and intercellular adhesion molecule-1 (ICAM-1) and vascular cell adhesion molecule (VCAM-1), which mediate firm adhesion and transmigration of leukocytes. The development of nanoparticulate contrast agents targeting these adhesion molecules is aimed at non-invasively detecting early atherogenic changes as well as active lesions.

One example to target E-selectin involved the generation of pegylated paramagnetic liposomes carrying an anti-E-selectin

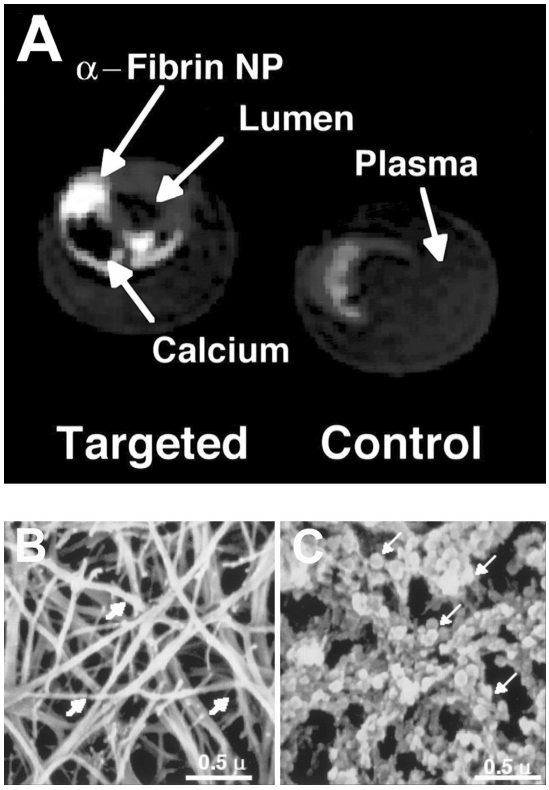

Figure 3. (A) Color-enhanced, fast gradient echo, T1-weighted, fat-suppressed, MR images at 1.5T of human endarterectomy specimen incubated with fibrin-targeted perfluorocarbon nanoparticles. The incubation of this specimen was performed in blood-free environment *ex-vivo*. Contrast enhancement (white) of a small fibrin deposit on a symptomatic ruptured plaque and calcium deposit (black). (B) Scanning electron micrographs (x 30,000) of control fibrin clot. (C) Fibrin-targeted paramagnetic nanoparticles bound to clot surface. Modified reprint with permission (34).

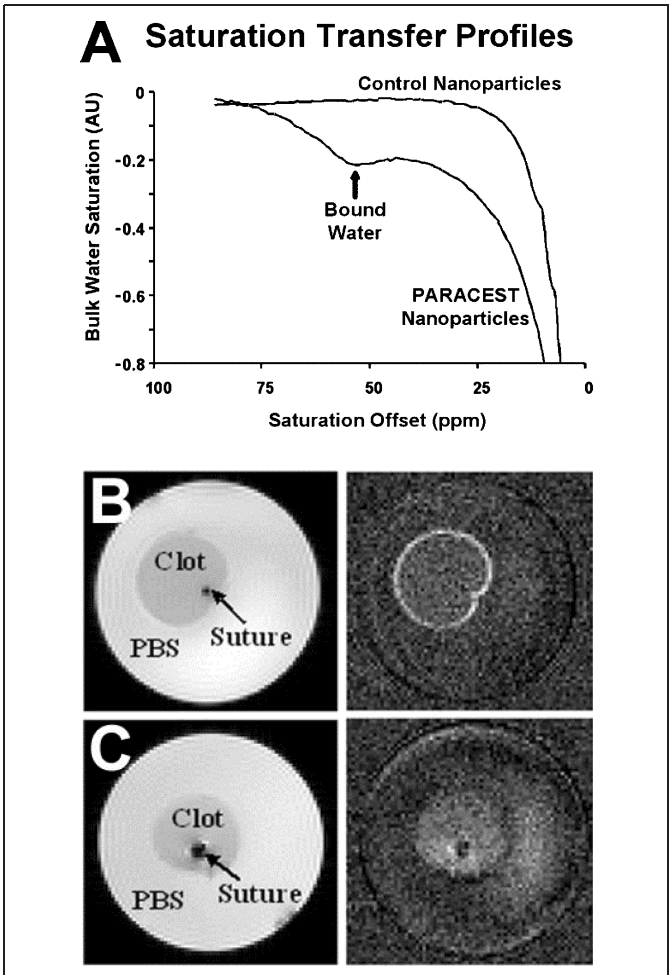

Figure 4. (A) Saturation profile of PARACEST nanoparticles depicting the saturation contrast effect at 52 ppm (arrow). Control nanoparticles show no such effect at this chemical shift. (Panel B) *In vitro* fibrin clot targeted with anti-fibrin PARACEST nanoparticles. Images collected with pre-saturation at -52 ppm. Subtraction images (right) show signal enhancement on the surface on the clot treated with PARACEST nanoparticles. (Panel C) No difference in signal intensity upon targeting with control nanoparticles. However, subtraction images (right) show no enhancement of the clot treated with control nanoparticles. Compared to control nanoparticles, the contrast to noise ratio at the clot surface was significantly higher for fibrin-targeted PARACEST nanoparticles (10.0 ± 1.0 vs. 2.2 ± 0.4: $p < 0.05$). Modified reprint with permission (44).

monoclonal antibody as targeting ligand (52). Human umbilical vein endothelial cells (HUVEC) were treated with the pro-inflammatory cytokine tumor necrosis factor α (TNFα) to up-regulate the expression of E-selectin and then incubated with the paramagnetic targeted liposomes. MRI microscopy at 6.3 T revealed the specific association of this liposomal contrast agent with the stimulated HUVEC. Subsequently, these targeted liposomes were injected into apoE$^{-/-}$ mice with induced neointimal lesions due to previously placed constrictive collars around the right carotid artery. The thickened right carotid vessel wall of mice injected with the liposomes showed a pronounced signal enhancement immediately after injection, which was sustained largely until 24 hours post injection, while no contrast enhancement was observed in the controls (53).

The expression of leukocyte adhesion molecules in inflamed vessels with activated endothelium in mice with experimental autoimmune encephalitis (a model of multiple sclerosis) has been detected with MRI using polymerized liposomes conjugated to biotinylated antibodies specific for ICAM-1 (54). In these early experiments, the brains were scanned *ex vivo* with high resolution MRI at 9.4T. T1-weighted images showed increased signal intensity in the brains of animals that had received the targeted liposomes as compared to non-targeted and good correlation with the pattern of ICAM-1 expression on immunohistology was observed.

Recently, using phage display, a peptide sequence of the very late antigen-4 (a known ligand for VCAM-1) was identified and conjugated with a monocrystalline magnetic nanoparticle (VINP-28) (55, 56). MR imaging in apoE$^{-/-}$ mice after systemic injection of VINP-28 nanoparticles revealed a decrease in signal intensity in the aortic root *in vivo* (55). This effect was blunted in mice treated with atorvastatin concordant with

less VCAM-1 expression on histological examination. In addition, human carotid endarterectomy specimen were incubated with VINP-28 *ex vivo*. After 24 hours, samples incubated with VINP-28 demonstrated a T2 reduction compared to saline incubated samples. The colocalization of VINP-28 with VCAM-1-expressing cells was confirmed with immunohistochemistry. The utility of dual-imaging is nicely illustrated in a study by the same group evaluating VCAM-1 expression via fluorescence and MRI. For this task, a corresponding peptide to VCAM-1 (VP) was coupled multivalently to a superparamagnetic fluorescent nanoparticle termed VNP (56). Twenty-four hours after administration of the VNP a decrease of signal intensity in the atherosclerotic aorta of apoE$^{-/-}$ mice was detected with MRI and further corroborated by epifluorescence imaging of Cy 5.5 in VNP (Figure 5).

MOLECULAR IMAGING OF THE INTIMA AND MEDIA

Inflammatory mechanisms couple dyslipidemia to formation of atherosclerotic lesions (48). Early events in atherogenesis are the expression of pro-inflammatory cytokines and lymphocyte and monocyte recruitment into the vascular wall. The accumulation of these cellular elements and of lipids is the single most important contributor to growing atheroma burden but also provides targets for molecular imaging. First, cells migrating into the atheroma can be labeled *in vivo* with nanoparticulate contrast agents, such as iron containing particles. Second, cells within the atheroma can be targeted, e.g., integrins on smooth cells. Third, cells that migrate into the atherosclerotic plaque can be labeled *ex vivo* and injected. This approach is particularly useful for stem cell labeling. Fourth, lipids such as modified LDL and HDL can be labeled and tracked into the atheroma. Fifth, apoptosis within atherosclerotic lesions offers a target for nanoparticle facilitated detection. Finally, a non-targeted gadolinium-based micelle forming nanoparticle Gadofluorine passively accumulates in atherosclerotic lesions secondary to the enhanced permeability effect.

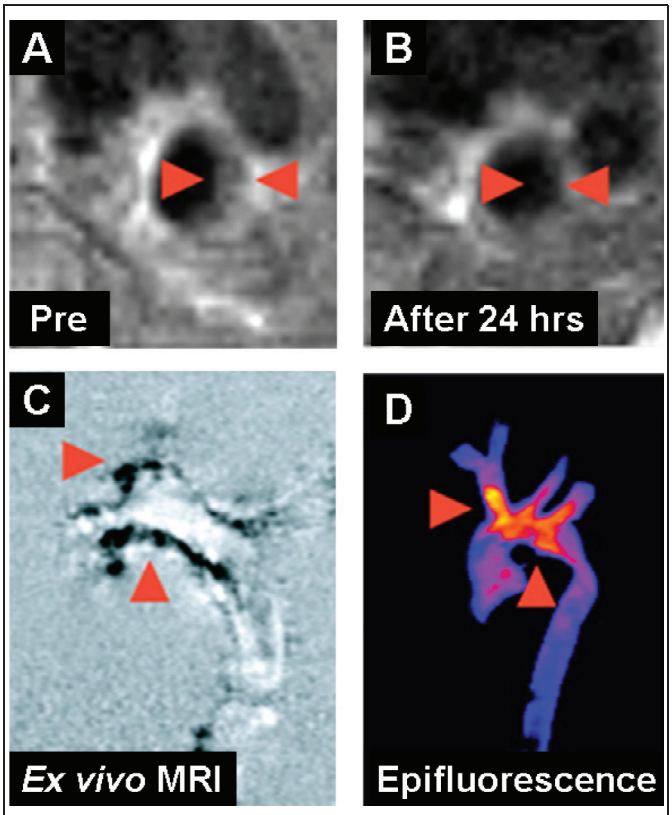

Figure 5. Dual MR and epifluorescence imaging of aortic atherosclerosis in cholesterol-fed apoE$^{-/-}$ mice. MR imaging of the descending aorta before (A) and 24 hours after (B) administration of superparamagnetic Cy 5.5 fluorescent-labeled and VCAM-1-targeted nanoparticles. (B) Decrease in signal intensity of the eccentrically thickened aortic wall (arrows) confirms successful targeting. (C) *Ex vivo* MRI depicts the extend of nanoparticle uptake. (D) Macroscopic epifluorescence imaging of Cy 5.5 in the nanoparticles. Modified reprint with permission (56).

Gadofluorine is a macrocyclic gadolinium contrast agent, which forms small micelles (~5 nm) in dilution secondary to their hydrophobic fluorinated side chain (57). In contrast to most molecular imaging agents, it is not specifically targeted. However, it has been shown to successfully detect atherosclerotic plaques in heritable hyperlipidemic rabbits (58, 59). This effect is thought to be due to the enhanced permeability effect, which is observed in atherosclerotic lesions (60).

In vivo *cell labeling/targeting*

Experimental animal studies have shown that USPIOs accumulate in sufficient quantities for MR detection in atherosclerotic plaques with high macrophage content (61–63). Subsequently, USPIOs were administered to humans prior to carotid endarterectomy (64,65). In some of these studies, the USPIOs (2.6 mg Fe/kg) were injected systemically, and MR imaging was performed prior to and 24 and 72 hours after injection (65). Signal decreases were observed in the vessel wall in 54% and 35% of the quadrants of the T2*-weighted MR images acquired after 24 and 72 hours, respectively. For those quadrants with changes, there was a significant signal decrease of 24% in regions of interest at 24 hours, but not after 72 hours. Histological and SEM analysis showed USPIOs to be localized predominantly within macrophages. Importantly, these USPIOs were detected in 75% of the ruptured and rupture-prone atheroma, but in 7% of the stable lesions, only. In addition to imaging atherosclerosis, magnetic nanoparticles have recently also been shown useful in the imaging of infarcted myocardium *in vivo* (66). In these experiments, magnetofluorescent CLIO-Cy5.5 nanoparticles were systemically injected into mice 48 hours after left coronary artery occlusion. An increase in contrast-to-noise ratio was observed in the anterolateral walls of the infarcted mice, and the fluorescence intensity was also significantly higher than in the sham operated controls.

A traditional disadvantage of using iron particles, which is the creation of dark or negative contrast on MR imaging, has been addressed with the development of off resonance methods for imaging the iron particles while suppressing background signal

(67–69). Lately, this approach was combined with conventional T2*-weighted gradient-echo sequences to image iron deposition with positive contrast (70). In these experiments, this GRASP sequence identified ferritin deposition both *in vitro* thrombi and *in vivo* crush-injured carotid arteries in rabbits. As a result of this positive contrast enhancement, this new technology may be of advantage to targeted nanoparticle applications delivering iron particles to the cells of interest.

Macrophages have also been specifically targeted taking advantage of the macrophage scavenger receptor (SR). Gd-carrying micelles were prepared by coupling biotinylated monoclonal rat anti-mouse antibody to murine SR-A types I and II and injected into 12 month old apoE$^{-/-}$ mice on a high fat diet for 6 months (71). *In vivo* MRI was performed with a 9.4T MRI and showed macrophage specific contrast uptake after 24 hours. The targeted immunomicelles yielded a 79% increase in signal intensity of atherosclerotic aortas in the apoE$^{-/-}$ mice compared with 34% using non-targeted micelles and no enhancement using Gd-DTPA.

Vascular smooth muscle cells (VSMC) are critical to the development of vascular stenosis following angioplasty procedures. Thus, inhibition of proliferation and migration of VSMC has long been a therapeutic goal. Initially, tissue factor was explored for imaging and potentially therapeutic nanoparticle applications. Tissue factor is available in the vascular media, and the inhibition of this factor had already been shown to inhibit restenosis (72). Perfluorocarbon nanoparticles were formulated with an anti-tissue factor antibody and binding to VSMC *in vitro* was imaged by ultrasound (73) and MRI (74, 75). Although tissue factor is present in the vascular wall, a time interval elapses until it becomes expressed on the cellular surface in response to vascular injury. To avoid this delay between the balloon overstretch injury and the incubation with molecularly targeted nanoparticles and thus decreasing the time of the interventional procedure, other potential molecular targets were investigated. Among those, collagen III and the $\alpha_v\beta_3$-integrin gained further interest. Collagen III is abundantly and immediately available in the medial and adventitial matrix, while $\alpha_v\beta_3$-integrin is constitutively expressed on VSMC, additionally upregulated in response to overstretch injury, and involved in smooth muscle cell migration and proliferation (76, 77). Paramagnetic perfluorocarbon nanoparticles were formulated with antibody to collagen III and a peptidomimetic against the $\alpha_v\beta_3$-integrin, respectively. These nanoparticle formulations were successfully tested *in vivo* in a pig-model of carotid artery balloon injury (78). Both nanoparticle emulsions bound to their targets and allowed the determination of localization and delineation of vascular injury morphology. However, the contrast to noise ratio was 4-fold higher for the $\alpha_v\beta_3$-integrin targeted nanoparticles as compared with the collagen III targeted particles as determined with T1-weighted MRI at 1.5T. This difference in contrast, which might have been due to relative density of available epitopes or differential probe avidity, led to the further pursuit of $\alpha_v\beta_3$-integrin targeted nanoparticles for therapeutic purposes.

Ex vivo *cell labeling*

Cross-linked iron oxide nanoparticles (CLIO) have been used to label T-lymphocytes *ex vivo* (79). Upon systemic injection, high-resolution MRI with a detection threshold of ~3 cells/voxel allowed the tracking of these cells in a mouse melanoma tumor model *in vivo*. Other protocols were developed using SPIO and polycationic transfection agents to label T-cells for *in vivo* tracking by MRI (80, 81).

Stem cell labeling

Early work included the labeling of pluripotent stem cells with iron-oxide particles. Successful incorporation of the imaging agent often proved difficult and required significant modification of the respective nanoparticle. In an early study, liposomes containing dextran-coated iron oxide particles were used for labeling human peripheral blood mononuclear cells *in vitro* (82). Liposome ingestion into the mononuclear cells was confirmed with electron microscopy and loss of signal in MR imaging was described. Another example is the targeting of transferrin receptors on stem cells with magnetically labeled nanoparticles (83). In these experiments, oligodendrocyte progenitor cells were incubated with nanoparticles, which had anti-transferrin-antibodies conjugated to the dextran cover of their iron-oxide cores. The tagged cells were transplanted into the spinal cord of myelin-deficient rats and cell migration followed using three-dimensional MR microscopy. In another study, an HIV-Tat peptide derivative was conjugated with iron-oxide particles to facilitate their ingestion into the progenitor cells (84). Labeling stem cells with iron oxide particles makes it possible to track them with MRI *in vivo*, but high intracellular levels of iron may cause radical formation and increase cytotoxicity. Thus, cationic liposomes were investigated for increased labeling efficiency in the absence of cytotoxic effects. In these experiments, sufficient intracellular uptake for detection and tracking of the stem cells by MRI *in vivo* was achieved at 100-fold lower concentrations of iron oxide (85).

Stem cell therapy has been demonstrated to restore injured myocardium and holds promise for the treatment of ischemic cardiomyopathy (86). This concept has subsequently been successful and proven safe in phase 1 clinical trials (87–89). However, a main limitation of this technology is given with the difficulty to non-invasively assess the engraftment and longitudinally follow survival of the cardiac stem cells. Typically, assessment of the left-ventricular ejection fraction has been used as a surrogate to determine the outcome. In one study, the left-ventricular ejection fraction was measured with CMR in 30 patients that received an intra-coronary injection of autologous bone marrow stem cells after an acute ST-segment elevation myocardial infarction and percutaneous coronary intervention (4.8 days prior to stem cell therapy) (89). The left-ventricular ejection fraction increased on average by 6.7% in the treatment group (0.7% in the control group; $p = 0.0026$) after 6 months. Interestingly, in a follow-up study on the same patients, no significant difference in left-ventricular ejection fraction was observed after 18 months

(90). While many factors may account for these findings, ability to non-invasively and longitudinally image stem-cell survival could lead to improvements in therapeutic strategies, i.e., initial injection of more stem cells, injection into more areas, or repeat injection. Another rationale for non-invasive imaging of stem cell engraftment and survival is given by the need to define their actual involvement in improved cardiac function. In many cases patients undergo percutaneous coronary interventions or coronary artery bypass surgery, which makes assessment of the specific contribution of the respective treatment difficult in the absence of stem cell imaging (91, 92). Several imaging strategies have been developed using radionuclide labeling (93), optical bioluminescence and positron emission tomography imaging (94–96). Using MRI, the engraftment of mesenchymal stem cells into the myocardium has been studied in a swine model of myocardial infarction (97). Magnetically labeled mesenchymal stem cells were injected into the myocardium, and contrast enhanced MRI at 1.5T demonstrated engraftment and allowed tracking of the labeled stem cells. In another study magnetically labeled mouse embryonic stem cells in a murine model of myocardial infarction were serially imaged over a 4 week period (98). CMR concomitantly allowed the assessment of left-ventricular function showing the dual capability of this technology to track stem cell survival and assess the therapeutic effect. While it has been shown that magnetically labeled stem cells maintain their ability to proliferate and differentiate (99,100), a limitation of this technology is the short-term persistence of the iron particles within the tissue even when the injected cells have undergone apoptosis. Thus, serial imaging may not adequately allow for the quantitation of surviving stem cells versus free iron particles or those that have been ingested by macrophages.

Other approaches to label stem cells utilized paramagnetic agents, such as cationic liposomes labeled with gadolinium (101). In fact, these particles were dual labeled with gadolinium and rhodamine for *in vivo* tracking with MRI and correlation by fluorescent microscopy. Blood derived endothelial progenitor cells (EPCs) hold a potential for increasing the neovascularization of ischemic sites. In order to determine their fate *in vivo*, EPCs have been labeled with a gadolinium-/europium-chelate as a dual (MRI and fluorescence) agent *in vitro* before injection under the mice kidney capsule or grafting on a subcutaneous Matrigel plug (102). Neovascular formation was observed *in vitro* experiments, and the labeled cells injected into mice were visualized *in vivo* for up to 14 days using 7T MRI.

The recent introduction of fluorine imaging allows the imaging of nanoparticulate agents containing fluorine (103-105). Since there is no significant amount of endogenous fluorine atoms present in the body, detection of the fluorine signal from these nanoparticles allows so-called hot-spot imaging without any background effects (Figure 6). This is especially important for stem cell tracking as the small number of these labeled cells causes only small changes in image contrast. Given its high specificity, ^{19}F imaging allows the quantification of particles delivered, and the images can be overlaid with those obtained with ^{1}H imaging to facilitate anatomical correlation. Perfluoropolyether (PFPE) containing nanoparticles were used to label phenotypically defined dendritic cells *ex vivo* and shown to enhance uptake by to 26-fold compared to free PFPE (106). These cationic nanoparticle transfected stem cells were then injected subcutaneously or intravenously into mice. At 6 hr post-injection, ^{19}F/^{1}H composite images showed the cells migrating and accumulating in local lymphnodes. Other investigators have labeled human umbilical cord blood derived mononuclear stem/progenitor cells with PFC nanoparticles containing PFOB for ^{1}H imaging or perfluoro-15-crown-5 ether for ^{19}F imaging, respectively (107). Importantly, the stem/progenitor cells readily internalized these PFC nanoparticles without aid of adjunctive labeling techniques (Figure 7). The cells remained functional, and ^{19}F signals were detected *in vivo* after both intravenous and intramuscular injection.

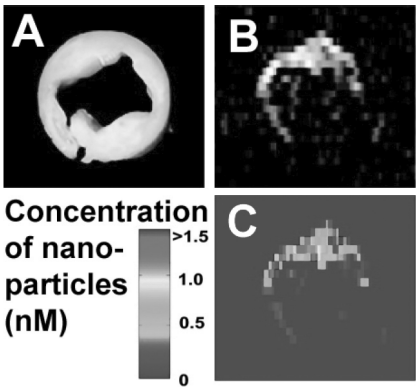

Figure 6. (A) Anatomical cross section of a human carotid endarterectomy specimen showing asymmetrical atherosclerosis. (B) ^{19}Fluorine image acquired at 4.7T depicts high signal intensity from fibrin-targeted crown ether nanoparticles that have bound along the luminal surface. (C) Nanoparticle concentration map allows the quantification of nanoparticles. Modified reprint with permission (105).

Lipid-labeling

HDL-like nanoparticles have been developed to take advantage of the role of HDL as a key player in reverse cholesterol transport by removing excess cholesterol from tissues, including atherosclerotic plaque (108, 109). HDL routinely crosses through the endothelial layer to enter and exit atherosclerotic plaque, making it an attractive 'shuttle' for very small nanoparticles. One of the first developed HDL-like nanoparticles (7–12 nm diameter) included isolated human HDL and a phospholipid-based GdDTPA contrast agent that becomes incorporated into the reconstituted HDL particle (110). These particles were injected intravenously into apoE$^{-/-}$ mice and imaged by MRI *in vivo*. Sequential MRI showed that the HDL-like nanoparticles localized predominantly at the atherosclerotic plaque by 24 hours after injection (Figure 8). After 48 hours, the intensity of the signal from the plaque decreased to a value similar to that obtained immediately after the injection. Importantly, the enhancement was also related

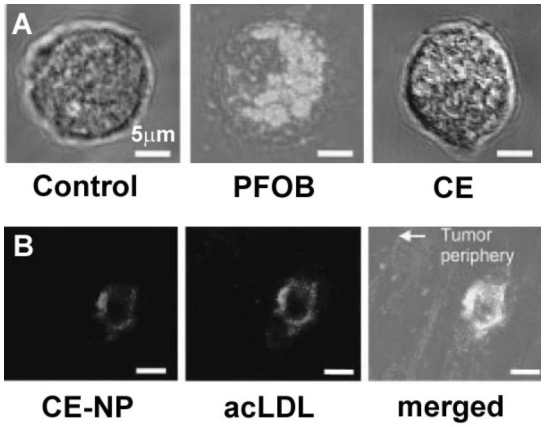

Figure 7. (Panel A) Confocal micrographs with simultaneous differential interference contrast imaging show control (left), cells containing nitro benzoxadiazole-labeled PFOB nanoparticles (middle), and cell cytosol accumulation of rhodamine-labeled crown ether (CE) nanoparticles. (Panel B) Umbilical cord blood-derived stem/progenitor cells containing CE nanoparticles (red) and acetylated LDL (green). Five days after intravenous injection, these cells are now localized in a vessel at the tumor periphery (mouse model of human breast carcinoma implanted 10 prior to stem cell injection). Modified reprint with permission (107).

to plaque composition showing higher signal intensity with higher cellularity as correlated with histology. In addition to these spherical HDL nanoparticles that contain core lipids and gadolinium, the same group of investigators has recently developed two types of discoidal nanoparticles (111). These particles were injected into the tail veins of 13 month old apoE$^{-/-}$ mice. MR imaging at 9.4T showed that both types of discoidal nanoparticles localized predominantly in atherosclerotic plaques and showed a time dependency with regards to plaque composition as determined by subsequent histological analysis. In these *in vivo* experiments, early contrast enhancement (24 hr) was observed in macrophage-rich plaques, whereas plaques with cholesterol crystals but fewer macrophages, showed late enhancement (72 hr). Complete wash-out of signal was observed by 48 hr and 96 hr, respectively. Confocal fluorescence microscopy revealed that the nanoparticles were internalized by macrophage/foam cells located primarily in the intimal layer.

Over-expression of LDL receptors on macrophages and other cells occurs in the hyperlipidemic atherogenic environment and allows increased ingestion of LDL during foam cell development. The highly selective binding of LDL to LDL receptors has generated interest to use LDL particles as a potential "shuttle" for nanoparticles into the cells of interest. Since LDL receptors are also over-expressed in some malignancies, early experiments have utilized tumor models. In these studies, a lipophilic GdDTPA derivative, conjugated to a fluorescent dye, was incubated briefly with LDL *in vitro* and injected into subcutaneously implanted B16 melanomas in mice (112). The *in vivo* uptake of the nanoparticle-labeled LDL lead to a 30% decrease in relaxation time (T1) in the tumor, compared to a 12% decrease in the liver of control mice lacking the LDL receptor.

APOPTOSIS

Programmed cell death is essential for tissue homeostasis. Enhanced levels of apoptosis may be observed in atherosclerotic lesions and contribute to plaque instability. Hence, the non-invasive visualization could yield important information on disease stage and progression. One of the first non-invasive detections of apoptosis utilized annexin V radiolabeled with technetium 99 m (113). Annexin V is an endogenous human protein with a high affinity for membrane bound phosphatidylserine, and the experimental strategy took advantage of the externalization of phosphatidylserine, a phospholipid normally restricted to the inner leaflet of the lipid bilayer of healthy cells. Subsequently, radiolabeled annexin V was used to non-invasively image apoptosis in areas of acute myocardial infarctions in humans (114), and fluorescent labeled annexin V was shown to image apoptotic membrane changes of single cardiomyocytes in the injured heart of living mice (115). In other studies, annexin V was labeled with the fluorophore Cy5.5 and served as an imaging probe for tumor apoptosis using near infrared fluorescence (NIRF) (116). The same group later synthesized a magneto/optical form of an annexin V CLIO nanoparticle for combined MR and NIRF imaging. In these *in vitro* experiments, apoptosis of camptothecin treated cells was detected with MRI and NIRF and correlated with FACS analyses (117). Another annexin A5-functionalized bimodal lipid-based contrast agent has been formulated to either incorporate iron oxide particles within pegylated micelles or Gd-DTPA-BSA lipids within the lipid bilayer of pegylated

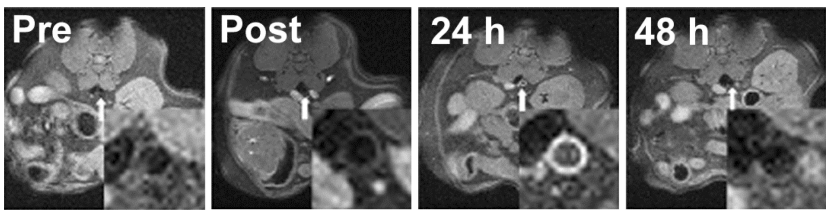

Figure 8. Sequential MR imaging of the abdominal aorta of atherosclerotic apoE$^{-/-}$ mice before and after intravenous injection of recombinant HDL-like nanoparticles (rHDL 4.36 μmol/kg). The contrast localized predominantly at the atherosclerotic plaque by 24 hours after the injection and cleared by 48 hours. Insets denote a magnification of the aortic region. Modified reprint with permission (110).

liposomes (118). The resulting nanoparticles were about 10 and 100 nm in diameter, respectively. Both agents allowed the detection *in vitro* of apoptotic cell pellets with MRI.

For MRI applications, a C2 domain of synaptotagmin I, which binds to anionic phospholipids in cell membranes of apoptotic cells, has been conjugated to superparamagnetic iron oxide nanoparticles SPIO (119). Non-invasive detection of apoptotic cells with MRI using such a targeted contrast agent has been shown *in vitro* with isolated apoptotic tumor cells, as well as *in vivo* in a murine lymphoma (EL4) tumor model (120).

MOLECULAR IMAGING OF ANGIOGENESIS

Growing atherosclerotic plaques eventually trigger an angiogenic response in the outer layer of the vessel wall. This occurs due to increased metabolic requirements and inability to meet this demand through diffusion from the inner vessel wall and the existing vasa vasorum in the outer wall. The angiogenic capillaries sprout out from the vasa vasorum but have been shown to have unique features (121–123). At the distal growth zone, the $\alpha_v\beta_3$-integrin is transiently expressed during the growth phase allowing for specific targeting of this integrin, which is otherwise not expressed on physiologically intact endothelium (124). Importantly, antagonists to the $\alpha_v\beta_3$-integrin promote tumor regression in animal (125) and human (126) tumor models via inhibition of angiogenesis. The $\alpha_1\beta_5$-integrin is another well characterized target for molecular imaging (127). In addition, integrin mediated direct cell adhesion to angiopoietins has been described (128). Hence, these receptors may provide a viable imaging target. Vascular endothelial growth factor (VEGF) is an important angiogenic factor induced by local hypoxia and interacts with tyrosine kinase receptors, which may be available for targeted imaging (129). Furthermore, the endothelial layer is not intact as in physiologic blood vessels but has enhanced permeability. These pores offer an opportunity for enhanced accumulation of targeted nanoparticle contrast agents.

The detection of angiogenesis was initially explored in tumor models, since angiogenesis is a crucial event in continuing tumor growth and reliable animal models exist for its study. In early experiments, $\alpha_v\beta_3$-specific antibodies (LM609) were conjugated to paramagnetic liposomes to facilitate MR imaging (130). The liposomes used in that study were 300-350 nm in diameter and contained 30% of the gadolinium-lipid resulting in a very high gadolinium payload per particle. Since these antibody-conjugated liposomes remain in the blood pool for extended periods, 24 hours were allowed for *in vivo* recirculation and binding to the $\alpha_v\beta_3$-integrin in the angiogenic vessels of rabbits subcutaneously implanted squamous cell carcinoma (V2). Imaged with a clinical 1.5 T MR scanner, this liposome formulation resulted in significant signal enhancement 24 hours after intravenous injection, and the signal location correlated with the $\alpha_v\beta_3$-integrin distribution as determined with immunohistology using the LM609 antibody. More recently, liposomes with a mean diameter of 150 nm were conjugated with an $\alpha_v\beta_3$-specific RGD peptide via PEG spacers and gadolinium was incorporated into the phospholipid double-layer. These liposomes were reported to bind to the proliferating endothelium in angiogenic vessels in a mouse tumor model as detected with MRI 35 minutes after systemic injection (131). Their distribution showed patterns associated with blood vessels as confirmed by histology. Competitive blocking with non-paramagnetic RGD liposomes led to a decrease of contrast enhanced voxels, confirming the specificity of binding. Others have modified quantum dots, i.e., semiconductor nanocrystals in a size range of 2-6 nm, for targeting of angiogenesis (132). These quantum dots were coated with paramagnetic and pegylated lipids resulting in a relaxivity of nearly 2000 $mM^{-1}s^{-1}$ per quantum dot. After covalently linking them with $\alpha_v\beta_3$-specific RGD peptides and incubation with endothelial cells in vitro, detection was possible with MRI and fluorescence.

Perfluorocarbon nanoparticles targeted against $\alpha_v\beta_3$-integrin have been demonstrated to detect angiogenesis in Vx-2 tumors implanted in rabbits (133), in a rabbit corneal micropocket model (134), and in a rabbit model of atherosclerosis (135) using T1-weighted MRI at 1.5T. In the atherosclerosis model, increased angiogenesis was detected as a 47% enhancement in MR signal averaged throughout the abdominal aortic wall in rabbits that had received a single intravenous injection of $\alpha_v\beta_3$-integrin targeted particles 2 hours earlier. Pretreatment of atherosclerotic rabbits with $\alpha_v\beta_3$-integrin targeted non-paramagnetic nanoparticles competitively blocked specific contrast enhancement of the $\alpha_v\beta_3$-integrin targeted paramagnetic agent. Histology confirmed the marked proliferation of angiogenic vessels within the aortic adventitia in comparison to sparse incidence of neovasculature in control animals.

Others have used macromolecular plasma proteins such as albumin and labeled it with biotin, a fluorescent tag, and Gd-DTPA for MR imaging (136). These labeled proteins extravasated from permeable blood vessels in a VEGF overexpressing tumor and were additionally 'chased' from the blood by intravenous administration of avidin. While this experimental model allowed the *in vivo* manipulation of the rate of clearance of the contrast media from the circulation, injection of large amounts of biotin avidin labeled contrast agents into humans may not be advantageous.

MR MONITORING OF THERAPEUTIC NANOPARTICULATE AGENTS

Microemulsions such as perfluorocarbon nanoparticles are particularly intriguing for drug delivery since they can be used to deliver drugs with poor water solubility, which is a feature of many drugs. Moreover, the large core of many of the microemulsions allows high payloads of drugs to be delivered.

Liposomes have been studied extensively to deliver mainly water-soluble drugs and several liposomal drug formulations are used in clinical applications, such as tumor therapy (137). Gene delivery and small interfering (si) RNA delivery with liposomes are novel applications that are developed mainly for tumor therapy as well (138–140).

Stenosis prevention

VSMC proliferate and migrate in response to vascular injury such as balloon-overstretch injury during angioplasty procedures to open occluded arteries. To prevent this restenosis response, nanoparticles have been targeted against epitopes in the vascular wall. Initially, tissue factor was targeted with perfluorocarbon nanoparticles formulated with an anti-tissue factor antibody. In addition to this targeting ligand, these nanoparticles contained doxorubicin or paclitaxel at 0, 0.2, or 2.0 mol% of the outer lipid layer (74). Upon a single 30 minute incubation of these nanoparticles with the VSMC in culture, the proliferation of VSMC was significantly inhibited for the next 3 days. High resolution T1-weighted MRI at 4.7T demonstrated the adherence of nanoparticles to the VSMC. Moreover, the perfluorocarbon core of the nanoparticles allowed the particle detection with ^{19}F MR spectroscopy. This technology provides an approach to quantify the amount of nanoparticles and thus drug payload delivered to the target. The MRI detection limit of sparse molecular epitopes when targeted with these nanoparticles has recently been modeled and validated *in vitro* (75,105).

For *in vivo* experiments exploring therapeutic effects of local drug delivery, nanoparticles were targeted against the $\alpha_v\beta_3$-integrin since this integrin is readily available for targeting immediately during the balloon overstretch injury and additionally upregulated in response to vascular injury. In a hypercholesteremic rabbit model of stenosis development following balloon overstretch injury, $\alpha_v\beta_3$-integrin targeted PFC nanoparticles that contained 0.4 mol% rapamycin as payload were incubated in the femoral artery segment immediately after injury for 5 minutes (141). Two weeks after this one-time treatment, the stenosis development was reduced 42% compared to control segments. These experiments have recently been extended to include dual-modality-imaging nanoparticles. $\alpha_v\beta_3$-integrin-targeted PFC-nanoparticles were labeled with ^{99m}Technetium as nuclear tracer and gadolinium-chelates for MR imaging. Immediately upon incubation of the nanoparticulate emulsion in the balloon-overstretch-injured femoral artery of cholesterol-fed NZW rabbits, SPECT/CT imaging allowed the confirmation of nanoparticle delivery as well as anatomical localization (Figure 9). Importantly, the quantification of the SPECT signal allows the calculation of the amount of nanoparticles delivered to the tissue and, thus, quantification of drug delivered. In these experiments, CMR served as a secondary imaging modality to image the nanoparticle delivery and anatomy. Hence, the dual-imaging modality employed was

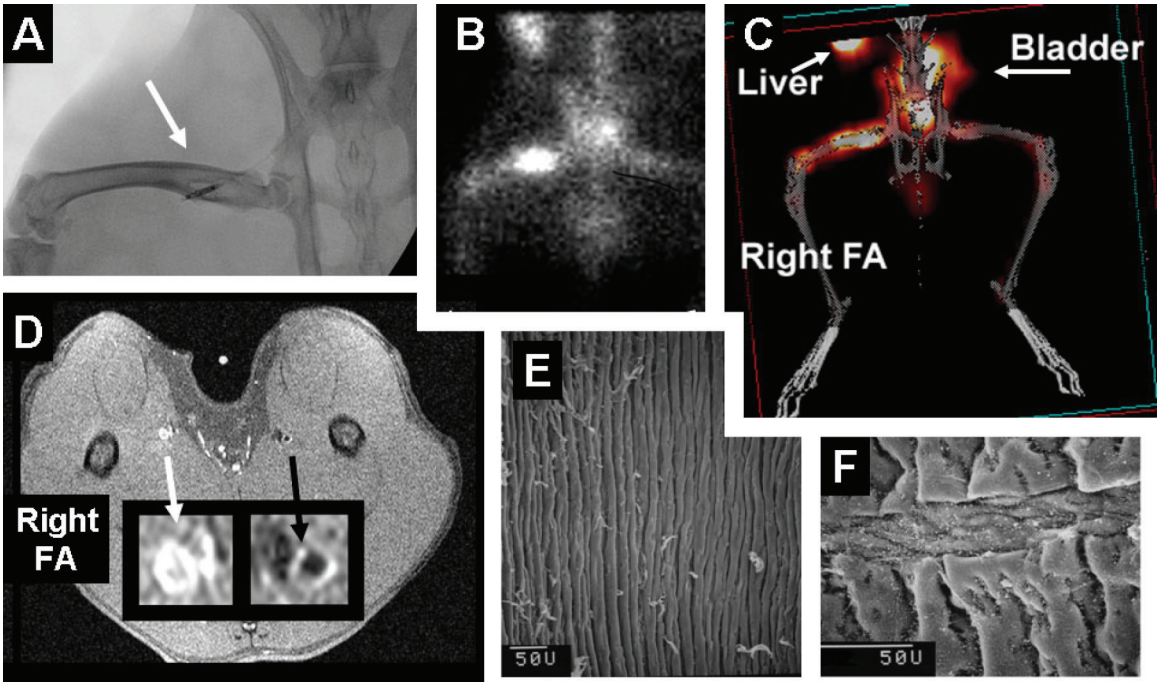

Figure 9. Dual-modality imaging and drug-delivery with PFC nanoparticles. (A) Balloon-overstretch-injury (arrow) of the right femoral artery prior to incubation with the $\alpha_v\beta_3$-integrin-targeted PFC nanoparticles (X-ray fluoroscopy). (B) The ^{99m}Tc-labeled nanoparticles emit strong signal as detected with SPECT. $\alpha_v\beta_3$-integrin-bound nanoparticles cause the hot spot in the right femoral artery while washed-out particles accumulate in the liver, and ^{99m}Tc is collected in the bladder for excretion. Importantly, systemically circulating nanoparticles do not accumulate in the left femoral artery, which was subjected to balloon overstretch-injury as well. (C) SPECT/CT image providing anatomical correlation of the nuclear signals and confirming the ^{99m}Tc-labeled nanoparticle delivery into the area of the injured right femoral artery. (D) CMR imaging with a conventional 1.5T MR system allows the detection and anatomical correlation of the $\alpha_v\beta_3$-integrin-bound nanoparticles in the right femoral artery due to labeling of these particles with gadolinium chelates. Again, the left femoral artery is void of any significant nanoparticle accumulation. (E and F) Scanning electron microscopy images of non-injured femoral artery endothelium (E), and histological proof of nanoparticle accumulation (small white dots) in the fissure of injured intima stretching through injured endothelium (F).

SPECT/MRI while CT was used purely for anatomical information. However, these PFC-nanoparticles can also be loaded with iodine making them amenable for direct SPECT/CT imaging showing the versatility of these nanoparticulate imaging agents.

Angiogenesis inhibition

Antagonists of the $\alpha_v\beta_3$-integrin have been shown to induce apoptosis of angiogenic blood vessels without affecting preexisting quiescent blood vessels (125). Perfluorocarbon nanoparticles targeted against the $\alpha_v\beta_3$-integrin in angiogenic vessels in a rabbit model of atherosclerosis have recently been successfully employed to deliver drugs into the angiogenic vessels, resulting in an anti-angiogenic effect (142). In these experiments, the intent was not to inhibit the $\alpha_v\beta_3$-integrin but rather use it as an available epitope for targeting of the nanoparticles to facilitate local drug delivery. As therapeutic agent fumagillin was integrated into the $\alpha_v\beta_3$-integrin targeted perfluorocarbon nanoparticles. Fumagillin is a naturally secreted antibiotic of the fungus *Aspergillus fumigatus fresenius* (143). Fumagillin and its synthetic analogues have been shown to inhibit angiogenesis (144) and entered clinical trials based on this finding long before the exact mechanism of action was established. The inhibition of angiogenesis entails endothelial cell cycle arrest in the late G_1 phase (145) and is mediated by the binding of fumagillin to a metalloprotease (methionine aminopeptidase; MetAP-2) (146). The fumagillin-mediated MetAP-2 inhibition has recently been shown to block noncanonical Wnt signaling, which plays a critical role in cell differentiation (147). Fumagillin initially was investigated for its potential therapeutic effects on tumor angiogenesis but, with the recognition of angiogenesis as contributor of atherosclerotic plaque growth, triggered interest for applications in cardiovascular therapies. The anti-angiogenic effects of the water-soluble fumagillin analogue TNP-470 (endostatin) was first reported in a model using apoE$^{-/-}$ mice (148). In these experiments, inhibition of atheroma progression was observed after 4 months. However, the drug had to be given every other day. To avoid frequent dosing and cumulative toxic effects (149), this drug has recently been evaluated for locally-targeted nanoparticle-facilitated delivery. A formulation of fumagillin-containing $\alpha_v\beta_3$-integrin targeted nanoparticles as well as non-drug containing $\alpha_v\beta_3$-integrin targeted control particles produced similar MRI signal enhancement at 1.5T (142). However, when $\alpha_v\beta_3$-integrin targeted nanoparticles were administered seven days later, significantly decreased MRI enhancement was observed among fumagillin treated rabbits as compared to control (Figure 10). This study illustrates the potential of combined molecular imaging and drug delivery with nanoparticles to non-invasively determine atherosclerotic burden, locally deliver drugs at a fraction of a systemic dose, and non-invasively quantify the treatment response at a later timepoint.

Nanoparticle technology has also been used to deliver genes to inhibit angiogenesis. In these experiments, a cationic polymerized liposomal nanoparticle was covalently coupled to a small organic $\alpha_v\beta_3$ ligand as well as the mutant *Raf* gene *ATP$^{\mu}$-Raf* (150). *ATPμ-Raf* blocks endothelial signaling and angiogenesis. Indeed, upon systemic injection into mice, sustained regression of the tumors was observed.

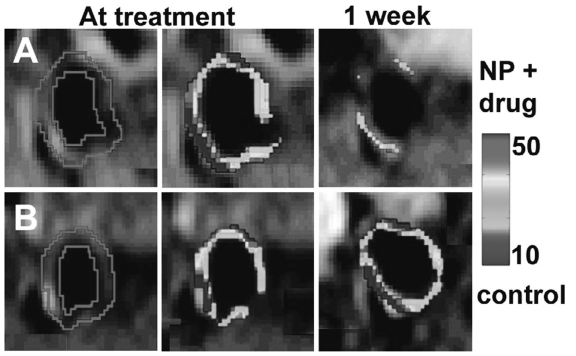

Figure 10. MRI at 1.5T of the abdominal aorta in cholesterol-fed rabbits showing outline of segmented areas of interest (left) and false-colored overlay of percent signal enhancement at time of treatment (middle) and one week after treatment. (Panel A) $\alpha_v\beta_3$-targeted nanoparticles with fumagillin. (Panel B) $\alpha_v\beta_3$-targeted nanoparticles without drug. Modified reprint with permission (142).

CONCLUSION

Atherosclerotic disease is not only a chronic condition with phases of acceleration but also potentially regression. The increasing prevalence of childhood obesity and other factors will likely cause atherosclerotic disease to become overt at younger ages, while improvement in treatment will cause patients to live longer. Thus, the life span during which imaging studies will need to be performed is increasing. At the same time, serial imaging to determine the need for, ideally prophylactic, interventions and to follow up on the outcome is paramount. Overall, this implies the requirement for more imaging studies per patient per life time than in the past. Among the currently available imaging modalities, MRI appears advantageous due to lack of both ionizing radiation and iodinated contrast agents. MRI depicts soft tissue with high spatial resolution, but has relatively low sensitivity. Targeted nanoparticulate MRI contrast agents effectively help to overcome this technical limitation. In the case of fluorine imaging, even single cells labeled with targeted contrast agents may be non-invasively imaged *in vivo*. Moreover, in the case of labeled stem cells, their movement may be non-invasively tracked, which may yield important information regarding successful engraftment.

Molecular imaging has the potential to non-invasively identify vulnerable plaque and, thus, may provide a timely risk assessment and guide further therapy to prevent acute coronary syndromes and the progression of vascular narrowing and thrombosis. Importantly, several molecularly targeted nanoparticle agents are currently being developed to locally provide treatments.

REFERENCES

1. Glagov S, Weisenberg E, Zarins C, Stankunavicius R, Kolettis G. Compensatory enlargement of human atherosclerotic coronary arteries. N Engl J Med 1987;316:1371–1375.
2. Farb A, Tang AL, Burke AP, Sessums L, Liang Y, Virmani R. Sudden Coronary Death : Frequency of active coronary lesions, inactive coronary lesions, and myocardial infarction. Circulation 1995;92:1701–1709.
3. Burke AP, Farb A, Malcom GT, Liang Y-h, Smialek J, Virmani R. Coronary risk factors and plaque morphology in men with coronary disease who died suddenly. N Engl J Med 1997;336:1276–1282.
4. Virmani R, Kolodgie FD, Burke AP, Farb A, Schwartz SM. Lessons from sudden coronary death: A comprehensive morphological classification scheme for atherosclerotic lesions. Arterioscler Thromb Vasc Biol 2000;20:1262–1275.
5. Arbustini E, Dal Bello B, Morbini P, Burke AP, Bocciarelli M, Specchia G, Virmani R. Plaque erosion is a major substrate for coronary thrombosis in acute myocardial infarction. Heart 1999;82:269–272.
6. Burke AP, Farb A, Malcom GT, Liang Y-h, Smialek J, Virmani R. Effect of risk factors on the mechanism of acute thrombosis and sudden coronary death in women. Circulation 1998;97:2110–2116.
7. Virmani R, Burke AP, Kolodgie FD, Farb A. Vulnerable plaque: the pathology of unstable coronary lesions. Journal of Interventional Cardiology 2002;15:439–446.
8. Burke AP, Kolodgie FD, Farb A, Weber DK, Malcom GT, Smialek J, Virmani R. Healed plaque ruptures and sudden coronary death: Evidence that subclinical rupture has a role in plaque progression. Circulation 2001;103:934–940.
9. Stegger L, Schaefers K, Kopka K, Wagner S, Hermann S, Kies P, Law M, Schober O, Schaefers M. Molecular cardiovascular imaging using scintigraphic methods. European Radiology 2007;17:1422–1432.
10. Wu JC, Bengel FM, Gambhir SS. Cardiovascular molecular imaging. Radiology 2007;244:337–355.
11. Spagnoli LG, Mauriello A, Sangiorgi G, Fratoni S, Bonanno E, Schwartz RS, Piepgras DG, Pistolese R, Ippoliti A, Holmes DR, Jr. Extracranial thrombotically active carotid plaque as a risk factor for ischemic stroke. JAMA 2004;292:1845–1852.
12. Barnett HJM, Taylor DW, Eliasziw M, Fox AJ, Ferguson GG, Haynes RB, Rankin RN, Clagett GP, Hachinski VC, Sackett DL, Thorpe KE, Meldrum HE, Spence JD, The north american symptomatic carotid endarterectomy trial C. benefit of carotid endarterectomy in patients with symptomatic moderate or severe stenosis. N Engl J Med 1998;339:1415–1425.
13. Collaborators NASCET. Beneficial effect of carotid endarterectomy in symptomatic patients with high-grade carotid stenosis. N Engl J Med 1991;325:445–453.
14. Hobson RW, Weiss DG, Fields WS, Goldstone J, Moore WS, Towne JB, Wright CB, Veterans affairs cooperative study G. Efficacy of carotid endarterectomy for asymptomatic carotid stenosis. N Engl J Med 1993;328:221–227.
15. Sitzer M, Muller W, Siebler M, Hort W, Kniemeyer HW, Jancke L, Steinmetz H. Plaque ulceration and lumen thrombus are the main sources of cerebral microemboli in high-grade internal carotid artery stenosis. Stroke 1995;26:1231–1233.
16. Carr S, Farb A, Pearce WH, Virmani R, Yao JST. Atherosclerotic plaque rupture in symptomatic carotid artery stenosis. Journal of Vascular Surgery 1996;23:755–766.
17. Cooke J. The pathophysiology of peripheral arterial disease: rational targets for drug intervention. Vascular Medicine 1997;2:227–230.
18. Ouriel K. Peripheral arterial disease. The Lancet 2001;358:1257–1264.
19. Dieter RS, Chu WW, Pacanowski JP, McBride PE, Tanke TE. The significance of lower extremity peripheral arterial disease. Clinical Cardiology 2002;25:3–10.
20. Williams G, Harrington D, Burdick J, White R. Mural thrombus of the aorta: an important, frequently neglected cause of large peripheral emboli. Annals of Surgery 1981;194:737–744.
21. Rossi PJ, Desai TR, Skelly CL, Curi MA, Glagov S, Schwartz LB. Paravisceral aortic thrombus as a source of peripheral embolization–Report of three cases and review of the literature. Journal of Vascular Surgery 2002;36:839–843.
22. Petty GW, Khandheria BK, Meissner I, Whisnant JP, Rocca WA, Sicks JD, Christianson TJH, O'Fallon WM, McClelland RL, Wiebers DO. Population-based study of the relationship between atherosclerotic aortic debris and cerebrovascular ischemic events. Mayo Clinic Proceedings 2006;81:609–614.
23. Fukumoto Y, Tsutsui H, Tsuchihashi M, Masumoto A, Takeshita A. The incidence and risk factors of cholesterol embolization syndrome, a complication of cardiac catheterization: a prospective study. Journal of the American College of Cardiology 2003;42:211–216.
24. Hansson GK. Inflammation, Atherosclerosis, and coronary artery disease. N Engl J Med 2005;352:1685–1695.
25. Kotani J-i, Mintz GS, Castagna MT, Pinnow E, Berzingi CO, Bui AB, Pichard AD, Satler LF, Suddath WO, Waksman R, Laird JR, Jr., Kent KM, Weissman NJ. Intravascular ultrasound analysis of infarct-related and non-infarct-related arteries in patients who presented with an acute myocardial infarction. Circulation 2003;107:2889–2893.
26. Hong M-K, Mintz GS, Lee CW, Kim Y-H, Lee S-W, Song J-M, Han K-H, Kang D-H, Song J-K, Kim J-J, Park S-W, Park S-J. Comparison of coronary plaque rupture between stable angina and acute myocardial infarction: A three-vessel intravascular ultrasound study in 235 patients. Circulation 2004;110:928–933.
27. Libby P, Theroux P. Pathophysiology of coronary artery disease. Circulation 2005;111:3481–3488.
28. Kolodgie FD, Burke AP, Farb A, Gold HK, Yuan J, Narula J, Finn AV, Virmani R. The thin-cap fibroatheroma: a type of vulnerable plaque: The major precursor lesion to acute coronary syndromes. Current Opinion in Cardiology 2001;16:285–292.
29. Davies MJ. Stability and instability: Two faces of coronary atherosclerosis: The paul dudley white lecture 1995. Circulation 1996;94:2013–2020.
30. Kolodgie FD, Gold HK, Burke AP, Fowler DR, Kruth HS, Weber DK, Farb A, Guerrero LJ, Hayase M, Kutys R, Narula J, Finn AV, Virmani R. Intraplaque hemorrhage and progression of coronary atheroma. N Engl J Med 2003;349:2316–2325.
31. Virmani R, Kolodgie FD, Burke AP, Finn AV, Gold HK, Tulenko TN, Wrenn SP, Narula J. Atherosclerotic plaque progression and vulnerability to rupture: Angiogenesis as a source of intraplaque hemorrhage. Arterioscler Thromb Vasc Biol 2005;25:2054–2061.
32. Lanza GM, Wallace KD, Scott MJ, Cacheris WP, Abendschein DR, Christy DH, Sharkey AM, Miller JG, Gaffney PJ, Wickline SA. A novel site-targeted ultrasonic contrast agent with broad biomedical application. Circulation 1996;94:3334–3340.
33. Lanza GM, Lorenz CH, Fischer SE, Scott MJ, Cacheris WP, Kaufmann RJ, Gaffney PJ, Wickline SA. Enhanced detection of thrombi with a novel fibrin-targeted magnetic resonance imaging agent. Academic Radiology 1998;5 Suppl. 1:S173–S176.
34. Flacke S, Fischer S, Scott MJ, Fuhrhop RJ, Allen JS, McLean M, Winter P, Sicard GA, Gaffney PJ, Wickline SA, Lanza GM. Novel MRI contrast agent for molecular imaging of fibrin: Implications for detecting vulnerable plaques. Circulation 2001;104:1280–1285.
35. Botnar RM, Perez AS, Witte S, Wiethoff AJ, Laredo J, Hamilton J, Quist W, Parsons EC, Jr., Vaidya A, Kolodziej A, Barrett JA, Graham PB, Weisskoff RM, Manning WJ, Johnstone MT. In vivo molecular imaging of acute and subacute thrombosis using

a fibrin-binding magnetic resonance imaging contrast agent. Circulation 2004;109:2023–2029.
36. Botnar RM, Buecker A, Wiethoff AJ, Parsons EC, Jr., Katoh M, Katsimaglis G, Weisskoff RM, Lauffer RB, Graham PB, Gunther RW, Manning WJ, Spuentrup E. In vivo magnetic resonance imaging of coronary thrombosis using a fibrin-binding molecular magnetic resonance contrast agent. Circulation 2004;110:1463–1466.
37. Spuentrup E, Fausten B, Kinzel S, Wiethoff AJ, Botnar RM, Graham PB, Haller S, Katoh M, Parsons EC, Jr., Manning WJ, Busch T, Gunther RW, Buecker A. Molecular magnetic resonance imaging of atrial clots in a swine model. Circulation 2005;112:396–399.
38. Sirol M, Fuster V, Badimon JJ, Fallon JT, Toussaint J-F, Fayad ZA. Chronic thrombus detection with in vivo magnetic resonance imaging and a fibrin-targeted contrast agent. Circulation 2005;112:1594–1600.
39. Dagher AP, Aletras A, Choyke P, Balaban RS. Imaging of urea using chemical exchange-dependent saturation transfer at 1.5T. Journal of Magnetic Resonance Imaging 2000;12:745–748.
40. Ward KM, Aletras AH, Balaban RS. A new class of contrast agents for MRI based on proton chemical exchange dependent saturation transfer (CEST). Journal of Magnetic Resonance 2000;143:79–87.
41. Guivel-Scharen V, Sinnwell T, Wolff SD, Balaban RS. Detection of proton chemical exchange between metabolites and water in biological tissues. Journal of Magnetic Resonance 1998;133:36–45.
42. Aime S, Delli Castelli D, Terreno E. Highly sensitive MRI chemical exchange saturation transfer agents using liposomes. Angewandte Chemie 2005;117:5649–5651.
43. Terreno E, Cabella C, Carrera C, Delli Castelli D, Mazzon R, Rollet S, Stancanello J, Visigalli M, Aime S. From spherical to osmotically shrunken paramagnetic liposomes: An improved generation of LIPOCEST MRI agents with highly shifted water protons. Angewandte Chemie 2007;119:984–986.
44. Winter PM, Cai K, Chen J, Adair CR, Kiefer GEK, Athey PS, Gaffney PJ, Buff CE, Robertson JD, Caruthers SD, Wickline SA, Lanza GM. Targeted PARACEST nanoparticle contrast agent for the detection of fibrin. Magnetic Resonance in Medicine 2006;56:1384–1388.
45. Aime S, Barge A, Castelli D, D., Fedeli F, Mortillaro A, Nielsen FU, Terreno E. Paramagnetic lanthanide(III) complexes as pH-sensitive chemical exchange saturation transfer (CEST) contrast agents for MRI applications. Magnetic Resonance in Medicine 2002;47:639–648.
46. Wolff SD, Balaban RS. Magnetization transfer contrast (MTC) and tissue water proton relaxation in vivo. Magn Reson Med 1989;10:135–144.
47. Querol M, Bogdanov Jr. A. Amplification strategies in MR imaging: Activation and accumulation of sensing contrast agents (SCAs). Journal of Magnetic Resonance Imaging 2006;24:971–982.
48. Libby P. Inflammation in atherosclerosis. Nature 2002;420:868–874.
49. Nakashima Y, Raines EW, Plump AS, Breslow JL, Ross R. Upregulation of VCAM-1 and ICAM-1 at atherosclerosis-prone sites on the endothelium in the ApoE-deficient mouse. Arterioscler Thromb Vasc Biol 1998;18:842–851.
50. Li H, Cybulsky MI, Gimbrone MA, Jr., Libby P. Inducible expression of vascular cell adhesion molecule-1 by vascular smooth muscle cells in vitro and within rabbit atheroma. Am J Pathol 1993;143:1551–1559.
51. Cybulsky MI, Gimbrone MA, Jr. Endothelial expression of a mononuclear leukocyte adhesion molecule during atherogenesis. Science 1991;251:788–791.
52. Mulder WJM, Strijkers GJ, Griffioen AW, vanBloois L, Molema G, Storm G, Koning GA, Nicolay K. A liposomal system for contrast-enhanced magnetic resonance imaging of molecular targets. Bioconjugate Chem. 2004;15:799–806.
53. Mulder WJM, Douma K, Koning GA, van Zandvoort MA, Lutgens E, Daemen MJ, Nicolay K, Strijkers GJ. Liposome-enhanced MRI of neointimal lesions in the ApoE-KO mouse. Magnetic Resonance in Medicine 2006;55:1170–1174.
54. Sipkins DA, Gijbels K, Tropper FD, Bednarski M, Li KCP, Steinman L. ICAM-1 expression in autoimmune encephalitis visualized using magnetic resonance imaging. Journal of Neuroimmunology 2000;104:1–9.
55. Nahrendorf M, Jaffer FA, Kelly KA, Sosnovik DE, Aikawa E, Libby P, Weissleder R. Noninvasive vascular cell adhesion molecule-1 imaging identifies inflammatory activation of cells in atherosclerosis. Circulation 2006;114:1504–1511.
56. Kelly KA, Allport JR, Tsourkas A, Shinde-Patil VR, Josephson L, Weissleder R. Detection of vascular adhesion molecule-1 expression using a novel multimodal nanoparticle. Circ Res 2005;96:327–336.
57. Staatz G, Nolte-Ernsting CC, Adam GB, Grosskortenhaus S, Misselwitz B, Bucker A, Gunther RW. Interstitial T1-weighted MR lymphography: lipophilic perfluorinated gadolinium chelates in pigs. Radiology 2001;220:129–134.
58. Barkhausen J, Ebert W, Heyer C, Debatin JF, Weinmann H-J. Detection of atherosclerotic plaque with gadofluorine-enhanced magnetic resonance imaging. Circulation 2003;108:605–609.
59. Sirol M, Itskovich VV, Mani V, Aguinaldo JGS, Fallon JT, Misselwitz B, Weinmann H-J, Fuster V, Toussaint J-F, Fayad ZA. Lipid-rich atherosclerotic plaques detected by gadofluorine-enhanced in vivo magnetic resonance imaging. Circulation 2004;109:2890–2896.
60. Colangelo S, Langille BL, Steiner G, Gotlieb AI. Alterations in endothelial F-Actin microfilaments in rabbit aorta in hypercholesterolemia. Arterioscler Thromb Vasc Biol 1998;18:52–56.
61. Ruehm SG, Corot C, Vogt P, Kolb S, Debatin JF. Magnetic resonance imaging of atherosclerotic plaque with ultrasmall superparamagnetic particles of iron oxide in hyperlipidemic rabbits. Circulation 2001;103:415–422.
62. Litovsky S, Madjid M, Zarrabi A, Casscells SW, Willerson JT, Naghavi M. Superparamagnetic iron oxide-based method for quantifying recruitment of monocytes to mouse atherosclerotic lesions in vivo: Enhancement by tissue necrosis factor-α, interleukin-1β, and interferon-γ. Circulation 2003;107:1545–1549.
63. Schmitz SA, Coupland SE, Gust R, Winterhalter S, Wagner S, Kresse M, Semmler W, Wolf K-J. Superparamagnetic iron oxide-enhanced mri of atherosclerotic plaques in watanabe hereditable hyperlipidemic rabbits. Investigative Radiology 2000;35:460–471.
64. Trivedi RA, U-King-Im J-M, Graves MJ, Cross JJ, Horsley J, Goddard MJ, Skepper JN, Quartey G, Warburton E, Joubert I, Wang L, Kirkpatrick PJ, Brown J, Gillard JH. In vivo detection of macrophages in human carotid atheroma: Temporal dependence of ultrasmall superparamagnetic particles of iron oxide-enhanced MRI. Stroke 2004;35:1631–1635.
65. Kooi ME, Cappendijk VC, Cleutjens KBJM, Kessels AGH, Kitslaar PJEHM, Borgers M, Frederik PM, Daemen MJAP, van Engelshoven JMA. Accumulation of ultrasmall superparamagnetic particles of iron oxide in human atherosclerotic plaques can be detected by in vivo magnetic resonance imaging. Circulation 2003;107:2453–2458.
66. Sosnovik DE, Nahrendorf M, Deliolanis N, Novikov M, Aikawa E, Josephson L, Rosenzweig A, Weissleder R, Ntziachristos V. Fluorescence tomography and magnetic resonance imaging of myocardial macrophage infiltration in infarcted myocardium in vivo. Circulation 2007;115:1384–1391.
67. Seppenwoolde J-H, Viergever MA, Bakker CJG. Passive tracking exploiting local signal conservation: The white marker

phenomenon. Magnetic Resonance in Medicine 2003;50:784–790.
68. Mani V, Briley-Saebo KC, Itskovich VV, Samber DD, Fayad ZA. Gradient echo acquisition for superparamagnetic particles with positive contrast (GRASP): Sequence characterization in membrane and glass superparamagnetic iron oxide phantoms at 1.5T and 3T. Magnetic Resonance in Medicine 2006;55:126–135.
69. Gilson WD, Stuber M, Hofmann LV, Kedziorek D, Karmarkar P, Bulte JW, Kraitchman DL. Novel magnetic resonance imaging technique for enhanced visualization of magnetically labeled mesenchymal stem cells and passive tracking of MR-compatible endovascular devices. Circulation 2005;112:U34–U34.
70. Mani V, Briley-Saebo KC, Hyafil F, Fayad ZA. Feasibility of in vivo identification of endogenous ferritin with positive contrast MRI in rabbit carotid crush injury using GRASP. Magnetic Resonance in Medicine 2006;56:1096–1106.
71. Amirbekian V, Lipinski MJ, Briley-Saebo KC, Amirbekian S, Aguinaldo JGS, Weinreb DB, Vucic E, Frias JC, Hyafil F, Mani V, Fisher EA, Fayad ZA. Detecting and assessing macrophages in vivo to evaluate atherosclerosis noninvasively using molecular MRI. PNAS 2007;104:961–966.
72. Oltrona L, Speidel CM, Recchia D, Wickline SA, Eisenberg PR, Abendschein DR. Inhibition of tissue factor–mediated coagulation markedly attenuates stenosis after balloon-induced arterial injury in minipigs. Circulation 1997;96:646–652.
73. Lanza GM, Trousil RL, Wallace KD, Rose JH, Hall CS, Scott MJ, Miller JG, Eisenberg PR, Gaffney PJ, Wickline SA. In vitro characterization of a novel, tissue-targeted ultrasonic contrast system with acoustic microscopy. J Acoust Soc Am 1998;104:3665–3672.
74. Lanza GM, Yu X, Winter PM, Abendschein DR, Karukstis KK, Scott MJ, Chinen LK, Fuhrhop RW, Scherrer DE, Wickline SA. Targeted antiproliferative drug delivery to vascular smooth muscle cells with a magnetic resonance imaging nanoparticle contrast agent: Implications for rational therapy of restenosis. Circulation 2002;106:2842–2847.
75. Morawski AM, Winter PM, Crowder KC, Caruthers SD, Fuhrhop RW, Scott MJ, Robertson JD, Abendschein DR, Lanza GM, Wickline SA. Targeted nanoparticles for quantitative imaging of sparse molecular epitopes with MRI. Magnetic Resonance in Medicine 2004;51:480–486.
76. Bishop GG, McPherson JA, Sanders JM, Hesselbacher SE, Feldman MJ, McNamara CA, Gimple LW, Powers ER, Mousa SA, Sarembock IJ. Selective $\alpha_v\beta_3$-Receptor blockade reduces macrophage infiltration and restenosis after balloon angioplasty in the atherosclerotic rabbit. Circulation 2001;103:1906–1911.
77. Corjay MH, Diamond SM, Schlingmann KL, Gibbs SK, Stoltenberg JK, Racanelli AL. $\alpha_v\beta_3$, $\alpha_v\beta_5$, and osteopontin are coordinately upregulated at early time points in a rabbit model of neointima formation. Journal of Cellular Biochemistry 1999;75:492–504.
78. Cyrus T, Abendschein DR, Caruthers SD, Harris TD, Glattauer V, Werkmeister JA, Ramshaw JAM, Wickline SA, Lanza GM. MR Three-dimensional molecular imaging of intramural biomarkers with targeted nanoparticles. Journal of Cardiovascular Magnetic Resonance 2006;8:535–541.
79. Kircher MF, Allport JR, Graves EE, Love V, Josephson L, Lichtman AH, Weissleder R. In vivo high resolution three-dimensional imaging of antigen-specific cytotoxic T-Lymphocyte Trafficking to Tumors Cancer Res 2003;63:6838–6846.
80. Arbab AS, Bashaw L, A., Miller BR, Jordan EK, Bulte JWM, Frank JA. Intracytoplasmic tagging of cells with ferumoxides and transfection agent for cellular magnetic resonance imaging after cell transplantation: methods and techniques. Transplantation 2003;76:1123–1130.
81. Frank JA, Miller BR, Arbab AS, Zywicke HA, Jordan EK, Lewis BK, Bryant LH, Jr., Bulte JWM. Clinically applicable labeling of mammalian and stem cells by combining superparamagnetic iron oxides and transfection agents. Radiology 2003;228:480–487.
82. Bulte JWM, Ma LD, Magin RL, Kamman RL, Hulstaert CE, Go KG, The TH, Leij LD. Selective MR imaging of labeled human peripheral blood mononuclear cells by liposome mediated incorporation of dextran-magnetite particles. Magnetic Resonance in Medicine 1993;29:32–37.
83. Bulte JWM, Zhang SC, van Gelderen P, Herynek V, Jordan EK, Duncan ID, Frank JA. Neurotransplantation of magnetically labeled oligodendrocyte progenitors: Magnetic resonance tracking of cell migration and myelination. PNAS 1999;96:15256–15261.
84. Lewin M, Carlesso N, Tung C-H, Tang X-W, Cory D, Scadden DT, Weissleder R. Tat peptide-derivatized magnetic nanoparticles allow in vivo tracking and recovery of progenitor cells. Nature Biotechnology 2000;18:410–414.
85. van den Bos EJ, Wagner A, Mahrholdt H, Thompson RB, Morimoto Y, Sutton BS, Judd RM, Taylor DA. Improved efficacy of stem cell labeling for magnetic resonance imaging studies by the use of cationic liposomes. Cell Transplantation 2003;12:743–756.
86. Orlic D, Kajstura J, Chimenti S, Jakoniuk I, Anderson SM, Li B, Pickel J, McKay R, Nadal-Ginard B, Bodine DM, Leri A, Anversa P. Bone marrow cells regenerate infarcted myocardium. Nature 2001;410:701–705.
87. Assmus B, Schachinger V, Teupe C, Britten M, Lehmann R, Dobert N, Grunwald F, Aicher A, Urbich C, Martin H, Hoelzer D, Dimmeler S, Zeiher AM. Transplantation of progenitor cells and regeneration enhancement in acute myocardial infarction (TOPCARE-AMI). Circulation 2002;106:3009–3017.
88. Perin EC, Dohmann HFR, Borojevic R, Silva SA, Sousa ALS, Mesquita CT, Rossi MID, Carvalho AC, Dutra HS, Dohmann HJF, Silva GV, Belem L, Vivacqua R, Rangel FOD, Esporcatte R, Geng YJ, Vaughn WK, Assad JAR, Mesquita ET, Willerson JT. Transendocardial, autologous bone marrow cell transplantation for severe, chronic ischemic heart failure. Circulation 2003;107:2294–2302.
89. Wollert KC, Meyer GP, Lotz J, Ringes Lichtenberg S, Lippolt P, Breidenbach C, Fichtner S, Korte T, Hornig B, Messinger D, Arseniev L, Hertenstein B, Ganser A, Drexler H. Intracoronary autologous bone-marrow cell transfer after myocardial infarction: the BOOST randomised controlled clinical trial. The Lancet 2004;364:141–148.
90. Meyer GP, Wollert KC, Lotz J, Steffens J, Lippolt P, Fichtner S, Hecker H, Schaefer A, Arseniev L, Hertenstein B, Ganser A, Drexler H. Intracoronary bone marrow cell transfer after myocardial infarction: eighteen months' follow-up data from the randomized, controlled BOOST (BOne marrOw transfer to enhance ST-elevation infarct regeneration) Trial. Circulation 2006;113:1287–1294.
91. Menasche P, Hagege AA, Vilquin J-T, Desnos M, Abergel E, Pouzet B, Bel A, Sarateanu S, Scorsin M, Schwartz K, Bruneval P, Benbunan M, Marolleau J-P, Duboc D. Autologous skeletal myoblast transplantation for severe postinfarction left ventricular dysfunction. Journal of the American College of Cardiology 2003;41:1078–1083.
92. Stamm C, Kleine HD, Westphal B, Petzsch M, Kittner C, Nienaber CA, Freund M, Steinhoff G. CABG and Bone Marrow Stem Cell Transplantation after myocardial infarction*. Thoracic and Cardiovascular Surgeon The 2004:152–158.
93. Aicher A, Brenner W, Zuhayra M, Badorff C, Massoudi S, Assmus B, Eckey T, Henze E, Zeiher AM, Dimmeler S. Assessment of the tissue distribution of transplanted human endothelial progenitor cells by radioactive labeling. Circulation 2003;107:2134–2139.
94. Wu JC, Chen IY, Sundaresan G, Min J-J, De A, Qiao J-H, Fishbein MC, Gambhir SS. Molecular imaging of cardiac cell transplantation in living animals using optical bioluminescence and positron emission tomography. Circulation 2003;108:1302–1305.

95. Cao F, Lin S, Xie X, Ray P, Patel M, Zhang X, Drukker M, Dylla SJ, Connolly AJ, Chen X, Weissman IL, Gambhir SS, Wu JC. In vivo visualization of embryonic stem cell survival, proliferation, and migration after cardiac delivery. Circulation 2006;113:1005–1014.

96. Wu JC, Spin JM, Cao F, Lin S, Xie X, Gheysens O, Chen IY, Sheikh AY, Robbins RC, Tsalenko A, Gambhir SS, Quertermous T. Transcriptional profiling of reporter genes used for molecular imaging of embryonic stem cell transplantation. Physiol. Genomics 2006;25:29–38.

97. Kraitchman DL, Heldman AW, Atalar E, Amado LC, Martin BJ, Pittenger MF, Hare JM, Bulte JWM. In vivo magnetic resonance imaging of mesenchymal stem cells in myocardial infarction. Circulation 2003;107:2290–2293.

98. Arai T, Kofidis T, Bulte JWM, de Bruin J, Venook RD, Berry GJ, Mcconnell MV, Quertermous T, Robbins RC, Yang PC. Dual in vivo magnetic resonance evaluation of magnetically labeled mouse embryonic stem cells and cardiac function at 1.5 t. Magnetic Resonance in Medicine 2006;55:203–209.

99. Tallheden T, Nannmark U, Lorentzon M, Rakotonirainy O, Soussi B, Waagstein F, Jeppsson A, Sjogren-Jansson E, Lindahl A, Omerovic E. In vivo MR imaging of magnetically labeled human embryonic stem cells. Life Sciences 2006;79:999–1006.

100. He G, Hao Z, Wei H, Yi W, Zhang X, Yue T, Wei Y, Hu S. In vivo imaging of bone marrow mesenchymal stem cells transplanted into myocardium using magnetic resonance imaging: A novel method to trace the transplanted cells. International Journal of Cardiology 2007;114:4–10.

101. Vuu K, Xie J, McDonald MA, Bernardo M, Hunter F, Zhang Y, Li K, Bednarski M, Guccione S. Gadolinium-rhodamine nanoparticles for cell labeling and tracking via magnetic resonance and optical imaging. bioconjugate chem. 2005;16:995–999.

102. Crich SG, Biancone L, Cantaluppi V, Duò D, Esposito G, Russo S, Camussi G, Aime S. Improved route for the visualization of stem cells labeled with a Gd-/Eu-Chelate as dual (MRI and fluorescence) agent. Magnetic Resonance in Medicine 2004;51:938–944.

103. Caruthers SD, Neubauer AM, Hockett FD, Lamerichs R, Winter PM, Scott MJ, Gaffney PJ, Wickline SA, Lanza GM. In vitro demonstration using 19F magnetic resonance to augment molecular imaging with paramagnetic perfluorocarbon nanoparticles at 1.5 Tesla. Invest Radiol 2006;41:305–12.

104. Fan X, River JN, Muresan AS, Popescu C, Zamora M, Culp RM, Karczmar GS. MRI of perfluorocarbon emulsion kinetics in rodent mammary tumours. Physics in Medicine and Biology 2006;51:211–220.

105. Morawski AM, Winter PM, Yu X, Fuhrhop RJ, Scott MJ, Hockett F, Robertson JD, Gaffney PJ, Lanza GM, Wickline SA. Quantitative "magnetic resonance immunohistochemistry" with ligand-targeted 19F nanoparticles. Magnetic Resonance Medicine 2004;52:1255–1262.

106. Ahrens ET, Flores R, Xu H, Morel PA. In vivo imaging platform for tracking immunotherapeutic cells. Nat Biotech 2005;23:983–987.

107. Partlow KC, Chen J, Brant JA, Neubauer AM, Meyerrose TE, Creer MH, Nolta JA, Caruthers SD, Lanza GM, Wickline SA. 19F magnetic resonance imaging for stem/progenitor cell tracking with multiple unique perfluorocarbon nanobeacons. FASEB J. 2007:fj.06-6505com.

108. Fielding CJ, Fielding PE. Molecular physiology of reverse cholesterol transport. J. Lipid Res. 1995;36:211–228.

109. Brewer HB, Jr., Remaley AT, Neufeld EB, Basso F, Joyce C. Regulation of plasma high-density lipoprotein levels by the ABCA1 transporter and the emerging role of high-density lipoprotein in the treatment of cardiovascular disease. Arterioscler Thromb Vasc Biol 2004;24:1755–1760.

110. Frias JC, Williams KJ, Fisher EA, Fayad ZA. Recombinant HDL-like nanoparticles: A specific contrast agent for mri of atherosclerotic plaques. J. Am. Chem. Soc. 2004;126:16316–16317.

111. Frias JC, Ma Y, Williams KJ, Fayad ZA, Fisher EA. Properties of a versatile nanoparticle platform contrast agent to image and characterize atherosclerotic plaques by magnetic resonance imaging. Nano Lett. 2006;6:2220–2224.

112. Li H, Gray BD, Corbin I, Lebherz C, Choi H, Lund-Katz S, Wilson JM, Glickson JD, Zhou R. MR and fluorescent imaging of low-density lipoprotein receptors. Academic Radiology 2004;11:1251–1259.

113. Blankenberg FG, Katsikis PD, Tait JF, Davis RE, Naumovski L, Ohtsuki K, Kopiwoda S, Abrams MJ, Darkes M, Robbins RC, Maecker HT, Strauss HW. In vivo detection and imaging of phosphatidylserine expression during programmed cell death. PNAS 1998;95:6349–6354.

114. Hofstra L, Liem IH, Dumont EA, Boersma HH, van Heerde WL, Doevendans PA, DeMuinck E, Wellens HJJ, Kemerink GJ, Reutelingsperger CPM, Heidendal GA. Visualisation of cell death in vivo in patients with acute myocardial infarction. The Lancet 2000;356:209–212.

115. Dumont EA, Reutelingsperger CPM, Smits JFM, Daemen MJAP, Doevendans PAF, Wellens HJJ, Hofstra L. Real-time imaging of apoptotic cell-membrane changes at the single-cell level in the beating murine heart. Nat Med 2001;7:1352–1355.

116. Petrovsky A, Schellenberger E, Josephson L, Weissleder R, Bogdanov A, Jr. Near-infrared fluorescent imaging of tumor apoptosis. Cancer Res 2003;63:1936–1942.

117. Schellenberger EA, Sosnovik D, Weissleder R, Josephson L. Magneto/Optical Annexin V, a multimodal protein. Bioconjugate Chem. 2004;15:1062–1067.

118. vanTilborg GAF, Mulder WJM, Deckers N, Storm G, Reutelingsperger CPM, Strijkers GJ, Nicolay K. Annexin A5-functionalized bimodal lipid-based contrast agents for the detection of apoptosis. Bioconjugate Chem. 2006;17:741–749.

119. Jung Hi, Kettunen MI, Davletov B, Brindle KM. Detection of apoptosis using the c2a domain of synaptotagmin I Bioconjugate Chem 2004;15:983–987.

120. Zhao M, Beauregard DA, Loizou L, Davletov B, Brindle KM. Non-invasive detection of apoptosis using magnetic resonance imaging and a targeted contrast agent. Nat Med 2001;7:1241–1244.

121. Battegay EJ. Angiogenesis: mechanistic insights, neovascular diseases, and therapeutic prospects. Journal of Molecular Medicine 1995;73:333–346.

122. Simons M. Angiogenesis: Where do we stand now? Circulation 2005;111:1556–1566.

123. Carmeliet P. Angiogenesis in health and disease. Nat Med 2003;9:653–660.

124. Brooks PC, Clark RA, Cheresh DA. Requirement of vascular integrin alpha v beta 3 for angiogenesis. Science 1994;264:569–571.

125. Brooks PC, Montgomery AMP, Rosenfeld M, Reisfeld RA, Hu T, Klier G, Cheresh DA. Integrin $\alpha_v\beta_3$ antagonists promote tumor regression by inducing apoptosis of angiogenic blood vessels. Cell 1994;79:1157–1164.

126. Brooks PC, Stromblad S, Klemke R, Visscher D, Sarkar FH, Cheresh DA. Antiintegrin alpha v beta 3 blocks human breast cancer growth and angiogenesis in human skin. Journal of Clinical Investigation 1995;96:1815–1822.

127. Kim S, Bell K, Mousa SA, Varner JA. Regulation of angiogenesis in vivo by ligation of integrin $\alpha_5\beta_1$ with the central cell-binding domain of fibronectin. Am J Pathol 2000;156:1345–1362.

128. Carlson TR, Feng Y, Maisonpierre PC, Mrksich M, Morla AO. Direct cell adhesion to the angiopoietins mediated by integrins. J. Biol. Chem. 2001;276:26516–26525.

129. Ferrara N, Gerber H-P, LeCouter J. The biology of VEGF and its receptors. Nat Med 2003;9:669–676.

130. Sipkins DA, Cheresh DA, Kazemi MR, Nevin LM, Bednarski MD, Li KC. Detection of tumor angiogenesis in vivo

by alphaVbeta3-targeted magnetic resonance imaging. Nature Medicine 1998;4:623-626.
131. Mulder WJM, Strijkers GJ, Habets JW, Bleeker EJW, van der Schaft DWJ, Storm G, Koning GA, Griffioen AW, Nicolay K. MR molecular imaging and fluorescence microscopy for identification of activated tumor endothelium using a bimodal lipidic nanoparticle. FASEB J. 2005;19:2008–2010.
132. Mulder WJM, Koole R, Brandwijk RJ, Storm G, Chin PTK, Strijkers GJ, deMelloDonega C, Nicolay K, Griffioen AW. Quantum dots with a paramagnetic coating as a bimodal molecular imaging probe. Nano Lett. 2006;6:1–6.
133. Winter PM, Caruthers SD, Kassner A, Harris TD, Chinen LK, Allen JS, Lacy EK, Zhang H, Robertson JD, Wickline SA, Lanza GM. molecular imaging of angiogenesis in nascent Vx-2 rabbit tumors using a novel $\alpha_v\beta_3$-targeted nanoparticle and 1.5 tesla magnetic resonance imaging. Cancer Res 2003;63:5838–5843.
134. Anderson SA, Rader RK, Westlin WF, Null C, Jackson D, Lanza GM, Wickline SA, Kotyk JJ. Magnetic resonance contrast enhancement of neovasculature with $\alpha_v\beta_z$-targeted nanoparticles. Magnetic Resonance in Medicine 2000;44:433–439.
135. Winter PM, Morawski AM, Caruthers SD, Fuhrhop RW, Zhang H, Williams TA, Allen JS, Lacy EK, Robertson JD, Lanza GM, Wickline SA. Molecular imaging of angiogenesis in early-stage atherosclerosis with $\alpha_v\beta_3$-integrin-targeted nanoparticles. Circulation 2003;108:2270–2274.
136. Dafni H, Gilead A, Nevo N, Eilam R, Harmelin A, Neeman M. Modulation of the pharmacokinetics of macromolecular contrast material by avidin chase: MRI, optical, and inductively coupled plasma mass spectrometry tracking of triply labeled albumin. Magnetic Resonance in Medicine 2003;50:904–914.
137. Torchilin VP. RECENT ADVANCES WITH LIPOSOMES AS PHARMACEUTICAL CARRIERS. Nature Reviews Drug Discovery 2005;4:145–160.
138. Matsuura M, Yamazaki Y, Sugiyama M, Kondo M, Ori H, Nango M, Oku N. Polycation liposome-mediated gene transfer in vivo. Biochimica et Biophysica Acta (BBA) - Biomembranes 2003;1612:136–143.
139. Brignole C, Pagnan G, Marimpietri D, Cosimo E, Allen TM, Ponzoni M, Pastorino F. Targeted delivery system for antisense oligonucleotides: a novel experimental strategy for neuroblastoma treatment. Cancer Letters 2003;197:231–235.
140. Sioud M, Sorensen DR. Cationic liposome-mediated delivery of siRNAs in adult mice. Biochemical and Biophysical Research Communications 2003;312:1220–1225.
141. Cyrus T, Caruthers SD, Allen JS, Williams TA, Fuhrhop RW, Harris TD, Wickline SA, Lanza GM. avb3-integrin-targeted paramagnetic nanoparticles deliver rapamycin into the vascular wall and inhibit stenosis following balloon injury. Circulation 2006;114:217–217.
142. Winter PM, Neubauer AM, Caruthers SD, Harris TD, Robertson JD, Williams TA, Schmieder AH, Hu G, Allen JS, Lacy EK, Zhang H, Wickline SA, Lanza GM. Endothelial $\alpha_v\beta_3$ Integrin-targeted fumagillin nanoparticles inhibit angiogenesis in atherosclerosis. Arterioscler Thromb Vasc Biol 2006;26:2103–2109.
143. McCowen M, Callender M, Lawlis J. Fumagillin (H-3), a new antibiotic with amebicidal properties. Science 1951;23:202–203.
144. Ingber D, Fujita T, Kishimoto S, Sudo K, Kanamaru T, Brem H, Folkman J. Synthetic analogues of fumagillin that inhibit angiogenesis and suppress tumour growth. Nature 1990;348:555–557.
145. Abe Ji, Zhou W, Takuwa N, Taguchi Ji, Kurokawa K, Kumada M, Takuwa Y. A Fumagillin Derivative Angiogenesis Inhibitor, AGM-1470, Inhibits activation of cyclin-dependent kinases and phosphorylation of retinoblastoma gene product but not protein tyrosyl phosphorylation or protooncogene expression in vascular endothelial cells. Cancer Res 1994;54:3407–3412.
146. Sin N, Meng L, Wang MQW, Wen JJ, Bornmann WG, Crews CM. The anti-angiogenic agent fumagillin covalently binds and inhibits the methionine aminopeptidase, MetAP-2. PNAS 1997;94:6099–6103.
147. Zhang Y, Yeh JR, Mara A, Ju R, Hines JF, Cirone P, Griesbach HL, Schneider I, Slusarski DC, Holley SA, Crews CM. A chemical and genetic approach to the mode of action of fumagillin. Chemistry & Biology 2006;13:1001–1009.
148. Moulton KS, Heller E, Konerding MA, Flynn E, Palinski W, Folkman J. Angiogenesis inhibitors endostatin or TNP-470 reduce intimal neovascularization and plaque growth in apolipoprotein E–deficient Mice. Circulation 1999;99:1726–1732.
149. Kruger E, Figg W. TNP-470: an angiogenesis inhibitor in clinical development for cancer. Expert Opinion on Investigational Drugs 2000;9:1383–1396.
150. Hood JD, Bednarski M, Frausto R, Guccione S, Reisfeld RA, Xiang R, Cheresh DA. tumor regression by targeted gene delivery to the neovasculature. Science 2002;296:2404–2407.
151. Suwa T, Ozawa S, Ueda M, Ando N, Kitajima M. Magnetic resonance imaging of esophageal squamous cell carcinoma using magnetite particles coated with anti-epidermal growth factor receptor antibody. International Journal of Cancer 1998;75:626–634.
152. Panyam J, Labhasetwar V. Biodegradable nanoparticles for drug and gene delivery to cells and tissue. Advanced Drug Delivery Reviews 2003;55:329–347.
153. Zhang Y, Calon F, Zhu C, Boado RJ, Pardridge WM. Intravenous nonviral gene therapy causes normalization of striatal tyrosine hydroxylase and reversal of motor impairment in experimental parkinsonism. Human Gene Therapy 2003;14:1–12.
154. Bulte JWM, Douglas T, Witwer B, Zhang S-C, Strable E, Lewis BK, Zywicke H, Miller B, van Gelderen P, Moskowitz BM, Duncan ID, Frank JA. Magnetodendrimers allow endosomal magnetic labeling and in vivo tracking of stem cells. Nat Biotech 2001;19:1141–1147.